Inorganic Chemistry
Cite This: Inorg. Chem. 2018, 57, 6349−6361
Article
pubs.acs.org/IC

Chromophore-Functionalized Phenanthro-diimine Ligands and Their Re(I) Complexes

Kristina S. Kisel,[†,‡] Toni Eskelinen,[†] Waqar Zafar,[†] Anastasia I. Solomatina,[‡] Pipsa Hirva,[†] Elena V. Grachova,[‡] Sergey P. Tunik,*[,‡] and Igor O. Koshevoy*[,†]

[†]University of Eastern Finland, Department of Chemistry, Joensuu 80101, Finland
[‡]St.Petersburg State University, Department of Chemistry, Universitetskii pr. 26, 198504 St. Petersburg, Russia

Supporting Information

ABSTRACT: A series of diimine ligands has been designed on the basis of 2-pyridyl-1*H*-phenanthro[9,10-*d*]imidazole (**L1**, **L2**). Coupling the basic motif of **L1** with anthracene-containing fragments affords the bichromophore compounds **L3**−**L5**, of which **L4** and **L5** adopt a donor−acceptor architecture. The latter allows intramolecular charge transfer with intense absorption bands in the visible spectrum (lowest λ_{abs} 464 nm (ε = 1.2 × 10^4 M^{-1} cm^{-1}) and 490 nm (ε = 5.2 × 10^4 M^{-1} cm^{-1}) in CH_2Cl_2 for **L4** and **L5**, respectively). **L1**−**L5** show strong fluorescence in a fluid medium (Φ_{em} = 22−92%, λ_{em} 370−602 nm in CH_2Cl_2); discernible emission solvatochromism is observed for **L4** and **L5**. In addition, the presence of pyridyl (**L1**−**L5**) and dimethylaminophenyl (**L5**) groups enables reversible alteration of their optical properties by means of protonation. Ligands **L1**−**L5** were used to synthesize the corresponding [Re(CO)$_3$X(diimine)] (X = Cl, **1**−**5**; X = CN, **1-CN**) complexes. **1** and **2** exhibit unusual dual emission of singlet and triplet parentage, which originate from independently populated $^1\pi\pi^*$ and ^{3}MLCT excited states. In contrast to the majority of the reported Re(I) carbonyl luminophores, complexes **3**−**5** display moderately intense ligand-based fluorescence from an anthracene-containing secondary chromophore and complete quenching of emission from the ^{3}MLCT state presumably due to the triplet−triplet energy transfer (^{3}MLCT → ^{3}ILCT).

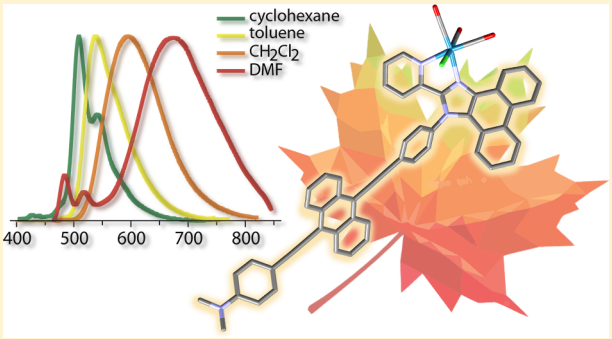

INTRODUCTION

Multichromophore compounds, i.e. species combining two or more photofunctional units, offer wide possibilities to manipulate the energy of electronic transitions on the molecular level and consequently within the bulk materials. Depending on the properties of the constituting blocks and the interplay between them, such molecules can be utilized for a diversity of light-harvesting, light-emitting, and charge transport purposes.[1−4] The efficiency of the targeted photophysical processes is defined by the dynamics of the excited state, which can be chemically tuned by proper molecular design.

An appealing approach to systems demonstrating unconventional photophysical behavior involves coupling of an organic chromophore with a transition-metal ion.[5] The presence of a d-block ion participating in the electronic transitions (e.g., metal to ligand or ligand to metal charge transfer, MLCT/LMCT) increases the number of accessible excited states. Furthermore, spin−orbit coupling induced by the heavy atom often activates fast intersystem crossing (ISC), leading to lower energy emissive states with triplet spin multiplicity.[6] Minimization of the electronic interaction between organic and metal-containing fragments in these molecules, e.g. by providing large spatial separation and/or by the lack of direct conjugation, may decouple the fluorescent and phosphorescent emitters to give dual singlet−triplet emission, suitable for ratiometric sensing[7−10] and panchromatic light generation.[11] In some cases even direct attachment of the metal center to the extended organic chromophore affords dual-emissive compounds[12−15] or complexes demonstrating prompt fluorescence[16] because of slow ISC rates. Nevertheless, the majority of the bi- or multichromophore metal−organic assemblies undergo efficient intramolecular energy transfer,[5,17−19] which makes these compounds fundamentally important for luminescent sensing,[20,21] singlet oxygen generation (photodynamic therapy),[22−24] and triplet−triplet annihilation upconversion.[25,26]

From a preparative viewpoint, one facile way to construct the metal−organic architectures relies on the coordination of the metal center to a presynthesized chromophore ligand. In this respect the rhenium(I) carbonyl diimine derivatives constitute an attractive and readily accessible class of photoactive complexes. These compounds play a noticeable role in bioimaging and photocatalysis[27−30] due to robust stereochemistry of the {Re(CO)$_x$(diimine)} (x = 2, 3) motif and its tailorability and rich photophysical behavior, dominated by

Received: February 15, 2018
Published: May 11, 2018

DOI: 10.1021/acs.inorgchem.8b00422
Inorg. Chem. 2018, 57, 6349−6361

the diimine-defined (MLCT or ligand-centered, LC) triplet excited state.[31]

Representative diimines containing extended aromatic systems or functionalized with an ancillary fluorophore, which are shown in Figure 1, have been successfully employed for the

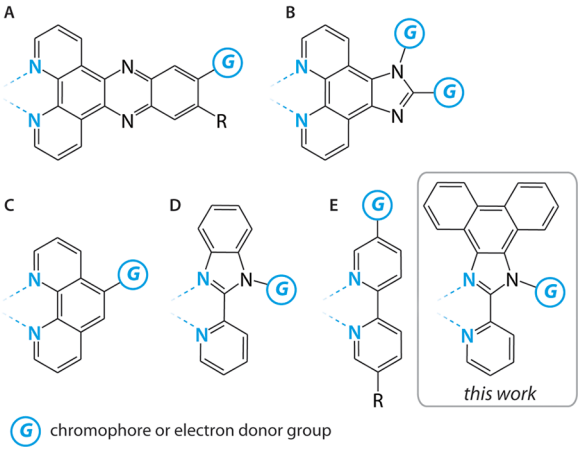

Figure 1. Representative chromophore diimine ligands used for the synthesis of rhenium(I) carbonyl complexes.

preparation of rhenium(I) carbonyl species. Extensive research efforts have been devoted to the compounds built on the family of dipyridophenazine ligands (A), the majority of which undergo formation of the dark (nonemissive) phenazine-localized triplet excited states of either ligand-centered (^{3}LC) or intraligand charge transfer (^{3}ILCT) nature.[32−36] On the other hand, Re(I) complexes based on phenanthroline-imidazole ligands (B) bearing electron donor (triphenylamine) groups display moderately intense MLCT/ILCT phosphorescence,[37] while for those with naphthalene and coumarine fragments luminescence is largely quenched due to the population of the low-lying ^{3}LC(chromophore) states from the ^{3}MLCT states.[38] A similar triplet−triplet energy transfer, which occurs in a "ping-pong" manner, has been found for phenanthroline (C)[39] and pyridyl-benzoimidazole (D)[40] ligands decorated with *N*-(1,10-phenanthroline)-4-(1-piperidinyl)naphthalene-1,8-dicarboximide and anthracene chromophores. In the case of phenanthrolines (C), bipyridines (E), and related ligands, anchoring the extended electron-rich groups results in intraligand charge transfer and a dominating triplet emission of ILCT and MLCT parentage.[41−45]

Recently, pyridyl-imidazoles fused with pyrene and phenanthrene motifs have been shown to serve as efficient chelating functions in Ru(II), Os(II), and Ir(III) complexes despite the steric hindrance introduced by the polyaromatic cores.[46,47] Inspired by this preparative success and rich photophysical behavior of Re(I) diimine carbonyl compounds, herein the coordinating pyridyl-phenanthroimidazole motif (Figure 1) has been employed for the construction of donor−acceptor bichromophore dyes. We have synthesized the derivatives of 1-phenyl- and 1-(4-bromophenyl)-2-(pyridin-2-yl)-1*H*-phenanthro[9,10-*d*]imidazole ligands (**L1** and **L2**) tailored to ethynyl-connected chromophores (anthracene, **L3**; diphenylamino-anthracene, **L4**; anthracene-ethynyl-dimethylaniline, **L5**), which were further used to generate the series of rhenium(I) chloro tricarbonyl complexes [Re(CO)$_3$X(diimine)] (X = Cl, **1**−**5**; X = CN, **1-CN**).

EXPERIMENTAL SECTION

General Comments. The solution ^{1}H and ^{1}H−^{1}H COSY NMR spectra were recorded on Bruker Avance 400 and AMX 400 spectrometers with chemical shifts referenced to residual solvent resonances. The infrared spectra were measured on a Shimadzu FTIR-8400S instrument. Mass spectra were recorded on a Bruker maXis II ESI-QTOF instrument in the ESI$^+$ and ESI$^-$ (for **2**−**5**) modes. Microanalyses were performed in the analytical laboratory of the University of Eastern Finland. The synthesis of the ligands (**L1**−**L5**) are provided in the Supporting Information.

Synthesis of Complexes Re(CO)$_3$Cl(L1−L5) (1−5). Pentacarbonylrhenium(I) chloride (100 mg, 0.28 mmol) and a stoichiometric amount of the corresponding ligand **L1**−**L5** (0.29 mmol) were suspended in ethanol (30 mL) and degassed by purging nitrogen for 15 min with stirring. The reaction mixture was refluxed for 5 h under a nitrogen atmosphere to give a yellow (**1**−**3**), orange (**4**), or red (**5**) suspension. The precipitate was collected, washed with ethanol and diethyl ether, dried, and purified by recrystallization.

Re(CO)$_3$Cl(L1) (1). Recrystallized by slow evaporation of its toluene solution to give bright yellow crystalline material (180 mg, 96%). IR (CH_2Cl_2, ν(CO) cm^{-1}): 2024s, 1921s, 1894s. ^{1}H NMR (DMSO-d_6, 298 K; δ): 9.34 (d, J_{HH} = 7.9 Hz, 1H), 9.21 (d, J_{HH} = 5.4 Hz, 1H), 9.01 (m, 2H), 8.14−7.83 (m, 7H), 7.72−7.61 (m, 3H), 7.42 (t, J_{HH} = 7.9 Hz, 1H), 7.02 (d, J_{HH} = 8.4 Hz, 1H), 6.80 (d, J_{HH} = 8.4 Hz, 1H). ESI$^+$ MS (*m*/*z*): 698.04 [M + Na]$^+$ (calcd 698.04). Anal. Calcd for $C_{29}H_{17}ClN_3O_3Re$: C, 51.44; H, 2.53; N, 6.21. Found: C, 51.51; H, 2.58; N, 6.25.

Re(CO)$_3$CN(L1) (1-CN). Complex **1** (100 mg, 0.15 mmol) and silver cyanide (22 mg, 0.16 mmol) were suspended in acetonitrile (60 mL), and the mixture was refluxed for 3 h under a nitrogen atmosphere in the absence of light. The suspension was cooled to room temperature and filtered through Celite, and the solvent was removed under reduced pressure. The solid residue was recrystallized by a gas-phase diffusion of diethyl ether into a dichloromethane solution of **1-CN** at room temperature to give a bright yellow crystalline material (90 mg, 90%). IR (CH_2Cl_2, ν(CO) cm^{-1}): 2024s, 1926s, 1914s. ^{1}H NMR (DMSO-d_6, 298 K; δ): 9.33 (dd, J_{HH} = 8.1 and 1.2 Hz, 1H), 9.23 (d, J_{HH} = 5.2 Hz, 1H), 9.03 (dd, J_{HH} = 8.1 and 5.2, 2H), 8.15 (m, 1H), 8.08 (dt, J_{HH} = 8.1 and 1.2 Hz, 1H), 8.02−7.92 (m, 4H), 7.88 (dd, J_{HH} = 7.7 and 1.2 Hz, 1H), 7.75−7.69 (m, 3H), 7.45 (dd, J_{HH} = 7.7 and 0.8 Hz, 1H), 7.04 (d, J_{HH} = 7.7 Hz, 1H), 6.83 (d, J_{HH} = 8.1 Hz, 1H). ESI$^+$ MS (*m*/*z*): 689.07 [M + Na]$^+$ (calcd 689.07). Anal. Calcd for $C_{30}H_{17}N_4O_3Re$: C, 53.97; H, 2.57; N, 8.39. Found: C, 53.79; H, 2.65; N, 8.31.

Re(CO)$_3$Cl(L2) (2). Recrystallized by a gas-phase diffusion of diethyl ether into a dichloromethane solution of **2** at room temperature to give a bright yellow crystalline material (200 mg, 95%). IR (CH_2Cl_2, ν(CO) cm^{-1}): 2025s, 1922s, 1895s. ^{1}H NMR (DMSO-d_6, 298 K; δ): 9.33 (d, J_{HH} = 8.3 Hz, 1H), 9.21 (d, J_{HH} = 5.5 Hz, 1H), 9.02 (m, 2H), 8.22−8.10 (m, 4H), 7.96 (t, J_{HH} = 7.8 Hz, 1H), 7.86 (t, J_{HH} = 7.8 Hz, 1H), 7.75−7.67 (m, 2H), 7.58 (dd, J_{HH} = 8.3 and 2.5 Hz, 1H), 7.51 (t, J_{HH} = 7.8 Hz, 1H), 7.06 (d, J_{HH} = 8.3 Hz, 1H), 6.91 (d, J_{HH} = 8.3 Hz, 1H). ESI$^-$ MS (*m*/*z*): 787.93 [M + Cl]$^-$ (calcd 787.93), 797.96 [M + HCOO]$^-$ (calcd 797.96). Anal. Calcd for $C_{29}H_{16}BrClN_3O_3Re$: C, 46.07; H, 2.13; N, 5.56. Found: C, 46.08; H, 2.15; N, 5.62.

Re(CO)$_3$Cl(L3) (3). Recrystallized by a gas-phase diffusion of diethyl ether into acetone/methanol solution of **3** at room temperature to give bright yellow crystalline material (236 mg, 96%). IR (CH_2Cl_2, ν(CO) cm^{-1}): 2025s, 1922s, 1894s. ^{1}H NMR (DMSO-d_6, 298 K; δ): 9.36 (d, J_{HH} = 8.1 Hz, 1H), 9.24 (d, J_{HH} = 5.3 Hz, 1H), 9.04 (m, 2H), 8.81 (s, 1H), 8.75 (d, J_{HH} = 8.1 Hz, 2H), 8.49 (dd, J_{HH} = 8.1 and 1.8 Hz, 1H), 8.40 (dd, J_{HH} = 8.1 and 1.8 Hz, 1H), 8.30 (dd, J_{HH} = 8.1 and 1.8 Hz, 1H), 8.24 (d, J_{HH} = 8.4 Hz, 2H), 8.16 (t, J_{HH} = 8.1 Hz, 1H), 7.98 (t, J_{HH} = 7.8 Hz, 1H), 7.88 (t, J_{HH} = 7.8 Hz, 1H), 7.80−7.65 (m, 7H), 7.54 (t, J_{HH} = 7.8 Hz, 1H), 7.21 (d, J_{HH} = 8.1 Hz, 1H), 7.04 (d, J_{HH} = 8.1 Hz, 1H). ESI$^-$ MS (*m*/*z*): 910.08 [M + Cl]$^-$ (calcd 910.08), 920.11 [M + HCOO]$^-$ (calcd 920.11). Anal. Calcd for $C_{45}H_{25}ClN_3O_3Re$: C, 61.60; H, 2.87; N, 4.79. Found: C, 61.80; H, 3.13; N, 4.87.

DOI: 10.1021/acs.inorgchem.8b00422
Inorg. Chem. 2018, 57, 6349−6361

Scheme 1. Synthesis of Ligands L1−L5[a]

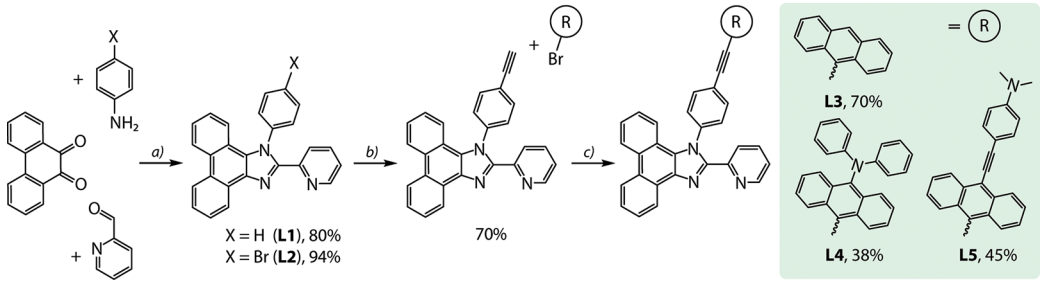

[a]Reagents and conditions: (a) NH_4OAc, toluene/AcOH, 68 °C, N_2, 12 h; (b) X = Br, HC_2SiMe_3, *n*-propylamine, $Pd(PPh_3)_4$, CuI, 57 °C, N_2, 48 h, then K_2CO_3 in THF/MeOH for 1 h; (c) *n*-propylamine, $Pd(PPh_3)_4$, CuI, 57 °C, N_2, 48 h.

*Re(CO)$_3$Cl(**L4**) (**4**).* Recrystallized by slow evaporation of its ethanol/dichloromethane solution at room temperature to give a bright orange crystalline material (280 mg, 96%). IR (CH_2Cl_2, ν(CO) cm^{-1}): 2025s, 1922s, 1894s. ^1H NMR (DMSO-d_6, 298 K; δ): 9.37 (d, J_{HH} = 7.8 Hz, 1H), 9.24 (d, J_{HH} = 4.6 Hz, 1H), 9.04 (m, 2H), 8.86 (d, J_{HH} = 8.4 Hz, 2H), 8.52 (d, J_{HH} = 8.2 Hz, 1H), 8.42 (d, J_{HH} = 8.2 Hz, 1H), 8.31 (d, J_{HH} = 8.2 Hz, 1H), 8.19−8.13 (m, 3H), 7.98 (t, J_{HH} = 7.8 Hz, 1H), 7.88 (t, J_{HH} = 7.8 Hz, 1H), 7.82−7.70 (m, 6H), 7.62 (m, 2H), 7.55 (t, J_{HH} = 7.8 Hz, 1H), 7.26−7.21 (m, 5H), 7.06−6.99 (m, 4H), 6.94 (t, J_{HH} = 7.4 Hz, 2H). ESI$^-$ MS (*m*/*z*): 1077.15 $[M + Cl]^-$ (calcd 1077.15), 1087.18 $[M + HCOO]^-$ (calcd 1087.18). Anal. Calcd for $C_{57}H_{34}ClN_4O_3Re$: C, 65.54; H, 3.28; N, 5.36. Found: C, 65.22; H, 3.39; N, 5.31.

*Re(CO)$_3$Cl(**L5**) (**5**).* Recrystallized by a gas-phase diffusion of diethyl ether into a dichloromethane/ethanol solution of **5** at room temperature to give a bright red crystalline material (274 mg, 96%). IR (CH_2Cl_2, ν(CO) cm^{-1}): 2025s, 1922s, 1894s. ^1H NMR (DMSO-d_6, 298 K; δ): 9.37 (d, J_{HH} = 8.1 Hz, 1H), 9.24 (d, J_{HH} = 5.3 Hz, 1H), 9.04 (m, 2H), 8.81 (m, 2H), 8.72 (m, 2H), 8.51 (m, 1H), 8.41 (m,1H), 8.30 (m, 1H), 8.16 (m, 1H), 7.98 (t, J_{HH} = 7.8 Hz, 1H), 7.90−7.69 (m, 10H), 7.54 (t, J_{HH} = 7.8 Hz, 1H), 7.22 (d, J_{HH} = 8.4 Hz, 1H), 7.04 (d, J_{HH} = 8.4 Hz, 1H), 6.84 (d, J_{HH} = 8.8 Hz, 2H), 3.03 (s, 6H). ESI$^-$ MS (*m*/*z*): 1053.15 $[M + Cl]^-$ (calcd 1053.15), 1063.18 $[M + HCOO]^-$ (calcd 1063.18). Anal. Calcd for $C_{55}H_{34}ClN_4O_3Re$: C, 64.73; H, 3.36; N, 5.49. Found: C, 64.4; H, 3.48; N, 5.61.

X-ray Structure Determinations. The crystals of **L1**, **L5**, **1**, **1-CN**, **2**, and **5** were immersed in cryo-oil, mounted in a Nylon loop, and measured at a temperature of 150 or 100 K (**L5**). The structures were determined on Bruker Kappa Apex II and Agilent Technologies Xcalibur diffractometers using Mo Kα (λ = 0.71073 Å) and Cu Kα (λ = 1.54184 Å) radiation, respectively. The APEX2[48] and CrysAlisPro[49] program packages were used for cell refinements and data reductions. A semiempirical or numerical absorption correction (SADABS[50] or SCALE3 ABSPACK[49]) was applied to all data. The structures were solved by direct methods using the SHELXS-2014[51] program with the WinGX[52] graphical user interface. Structural refinements were carried out using SHELXL-2014.[51] The crystallization solvent molecules in **1-CN** could not be resolved unambiguously; their contribution to the calculated structure factors was taken into account by using a SQUEEZE[53] routine of PLATON.[54] The missing solvent was not taken into account in the unit cell content.

All non-H atoms were anisotropically refined, and all hydrogen atoms were positioned geometrically and constrained to ride on their respective parent atoms with C−H = 0.89−0.99 Å and U_{iso} = 1.2−1.5U_{eq}(parent atom). The crystallographic details are summarized in Table S1.

Photophysical Measurements. Freshly distilled solvents (cyclohexane, toluene, dioxane, chlorobenzene, *o*-dichlorobenzene, dichloromethane, dimethylformamide, and acetonitrile) were used for the solution experiments. For complexes **1**−**5**, all solutions were carefully degassed before lifetime and quantum yield measurements by three "freeze−pump−thaw" cycles. UV−vis absorption spectra were recorded on a Shimadzu UV-1800 spectrophotometer. The excitation and emission spectra in solution were measured on a HORIBA FluoroMax-4 spectrofluorometer. Lifetimes were monitored on a HORIBA Scientific FluoroLog-3 spectrofluorometer. The emission quantum yields were determined by the comparative method[55] using coumarin 102 in ethanol (Φ_r = 0.764) as a standard with the refraction indexes of dichloromethane and ethanol equal to 1.42 and 1.36, respectively. The uncertainties of the quantum yield determinations were in the range of ±5% (an average of three measurements).

Computational Details. Electronic structure calculations were performed with the Gaussian 16 program package[56] within the framework of DFT/TD-DFT using the PBE0[57,58] hybrid density functional. A 6-311G+(d) basis set was used for the calculations involving pure ligands, while a def2-TZVPPD/6-311G(d) (Re/other atoms) basis set was used for the rhenium complexes.[59] The natures of the stationary points were confirmed by calculating the vibrational frequencies for the optimized S_0, S_1, and T_1 geometries. Calculations were performed in dichloromethane solvent using the C-PCM method.[60,61] Ground state S_0 optimizations were also performed under vacuum for comparison between X-ray structures.

RESULTS AND DISCUSSION

Synthesis and Characterization. The family of chelating ligands based on a 2-pyridyl-1*H*-phenanthro[9,10-*d*]imidazole core was prepared according to the reaction sequence summarized in Scheme 1. The 1-phenyl (**L1**)[47] and 1-(4-bromophenyl) (**L2**) derivatives were synthesized in good yields (80% and 94%, respectively) by the Debus−Radziszewski method starting from phenanthrene-9,10-dione, 2-pyridinecarboxaldehyde, and the corresponding aniline (see the Supporting Information for the experimental details). The subsequent two-step Sonogashira cross-coupling allows for the conversion of Br-aryl intermediate **L2** into the anthracene-functionalized compounds, which were isolated in moderate yields (38−70%) as yellow (**L3**, **L4**) and red (**L5**) crystalline solids, soluble in common organic solvents.

The ESI$^+$-MS of **L1**−**L5** display the dominating signals corresponding to the protonated molecular ions at *m*/*z* 372.15, 450.05, 572.21, 739.28, and 715.28, respectively (Figure S1, Supporting Information). The ^1H NMR spectra of these compounds display well-resolved multiplets in the aromatic region (Figure S2), which were assigned on the basis of 2D $^1H-^1H$ COSY experiments; their multiplicites and relative intensities are completely compatible with the structural patterns shown in Scheme 1.

The structures of **L1** and **L5** were established by XRD analysis (Figure 2 and Figure S3). Their molecular arrangements found in the solid state are in agreement with the spectroscopic data obtained in solution. The phenanthroimidazole core in both ligands is nearly flat, as well as the anthracenyl motif in **L5**.

DOI: 10.1021/acs.inorgchem.8b00422
Inorg. Chem. 2018, 57, 6349−6361

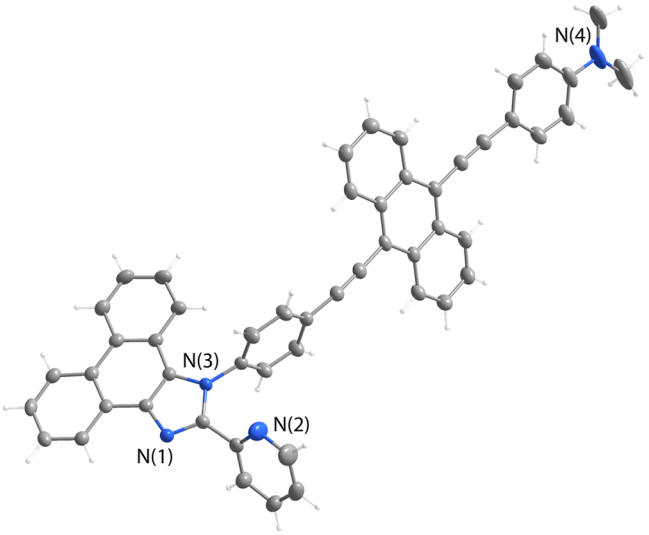

Figure 2. Molecular view of ligand **L5** (thermal ellipsoids are shown at the 50% probability level).

Scheme 2. Synthesis of Complexes 1−5[a]

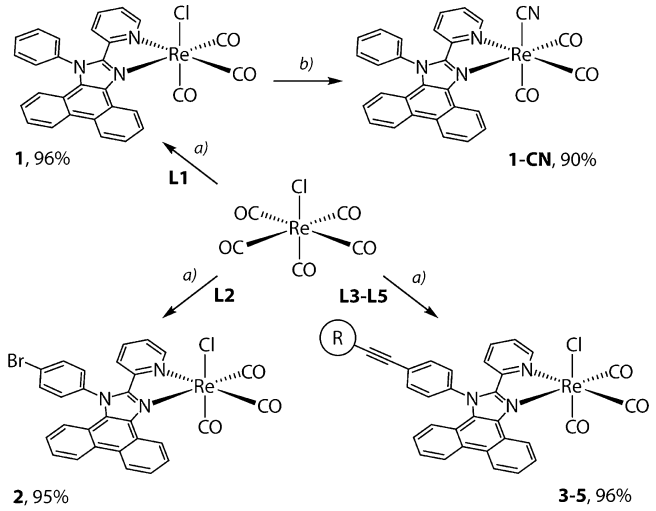

[a]Reagents and conditions: (a) EtOH, reflux, 5 h, N_2; (b) AgCN, MeCN, reflux, 3 h, N_2.

The planes of N(3)-bound phenyl(ene) rings in **L1** and **L5** are almost perpendicular to those of the imidazole fragment (the angles are 80 and 90° for **L1** for two independent molecules and 85° for **L5**), indicating that the conjugation between the polyaromatic moieties in chromophore-functionalized ligands **L3−L5** is most probably disrupted.

Despite the fact that the NMR data suggest unrestricted rotation of the C_6H_4 ring around the N(3)−carbon bond in solution at room temperature, it is reasonable to propose that the preferable conformation in the fluid medium corresponds to that found in the crystal due to the minimized intramolecular H−H repulsion. This conclusion is also supported by the computational analysis of the optimized geometries (Supporting Information). The crystal packing of **L5** reveals extensive intermolecular interactions (Figure S4), which evidently cause visible bending of the extended $-C_6H_4-C_2-An-C_2-C_6H_4-$ fragment.

The coordinating ability of the pyridyl-imidazole chelating moiety, fused with sterically demanding polyaromatic systems (phenanthrene, pyrene), has been successfully demonstrated for some late-transition-metal ions (Ir(III), Os(II), Ru(II)).[46,47,62] Similarly, ligands **L1−L5** can be employed for binding the $\{Re(CO)_3Cl\}$ fragment to give the complexes **1−5**, which belong to the family of well-known $[Re(CO)_3Cl(diimine)]$ species (see Scheme 2).

Compounds **1−5** were synthesized in high yields following the established procedures.[34,63] In the case of **1** bearing ligand **L1**, the chloride ion was substituted for the cyanide by reacting **1** with a stoichiometric amount of AgCN. Molecular structures of crystallographically characterized complexes **1**, **1-CN**, **2** and **5** are shown in Figure 3 and Figures S5 and S6; the relevant experimental details and selected bond distances and angles given in Tables S1 and S2.

The rhenium ions in these complexes adopt a pseudo-octahedral coordination geometry typical for the related tricarbonyl diimine species, with the N(1)−Re(1)−N(2) angles ranging from 73.95 to 74.25°. The steric hindrance introduced by the bulky phenanthrene moiety is expected to cause a strong repulsion between the equatorial C(2)O(2) ligand and the aromatic H−C group. This results in a significant displacement of the metal center from the plane of polycyclic NN′ motif (Figure 3); similarly to compounds with benzoquinoline ligands,[64] the dihedral angles between the planes of the Re(1), C(1), and C(2) atoms and of the imidazolyl ring are equal to 34.3° (**1**), 41.6° (**1-CN**), 27.5° (**2**), and 34.8° (**5**). In addition, the observed distortions systematically lead to the elongation of the $Re(1)-N_{imi}(1)$ bonds with respect to $Re(1)-N_{py}(2)$ distances (Table S2), which is in contrast to congener Re(I) complexes with pyridyl-imidazole ligands.[65−67]

Not surprisingly, compounds **1**, **1-CN**, **2**, and **5** display extensive $\pi-\pi$, π-C≡C. and CH-π intermolecular interactions (Figures S5 and S6), which essentially influence the crystal packing and might further increase the angle between the diimine backbones and the equatorial planes of the complexes, simultaneously inducing some curvature of the polyaromatic systems.

The spectroscopic data recorded for complexes **1−5** and **1-CN** in solution are compatible with the structures depicted in Scheme 2 and the results of the XRD analysis. The IR spectra of chloro tricarbonyl species **1−5** in the CO stretching region are nearly identical and show three strong bands at ca. 2025, 1922, and 1895 cm^{-1}, which correspond to *fac*-$M(CO)_3$ fragments lacking 3-fold symmetry.[43,68] The lower energy CO vibrations for **1-CN** are somewhat shifted to higher frequencies (2024, 1926, and 1914 cm^{-1}), which can be attributed to the substitution of the Cl^- for the CN^- ligand with a stronger π-accepting character.

The ESI-MS of **1−5** and **1-CN** reveal the signals $[\mathbf{1} + Na]^+$, $[(\mathbf{1\text{-}CN}) + Na]^+$ and $[(\mathbf{2-5}) + Cl]^-/[(\mathbf{2-5}) + HCOO]^-$ ions with the isotopic patterns, which fit completely the calculated patterns (Figure S7). The ^1H NMR spectra of these complexes contain well-resolved sets of resonances, which indicate a stereochemically rigid molecular arrangement under ambient conditions. The complete illustrative assignment, performed for **2** on the basis of the $^1H-^1H$ COSY and NOESY experiments (Figure S8), confirms that the solid-state structure remains unchanged in solution, including the preferential orientation of the imidazolyl-*N*-connected phenylene ring due to the restricted rotation around the $N(3)-C_6H_4$ bond.

Photophysical Properties and Theoretical Analysis. *Ligands L1−L5.* Compounds **L1−L5** contain extended aromatic motifs (phenanthrene (phen) and secondary

DOI: 10.1021/acs.inorgchem.8b00422
Inorg. Chem. 2018, 57, 6349−6361

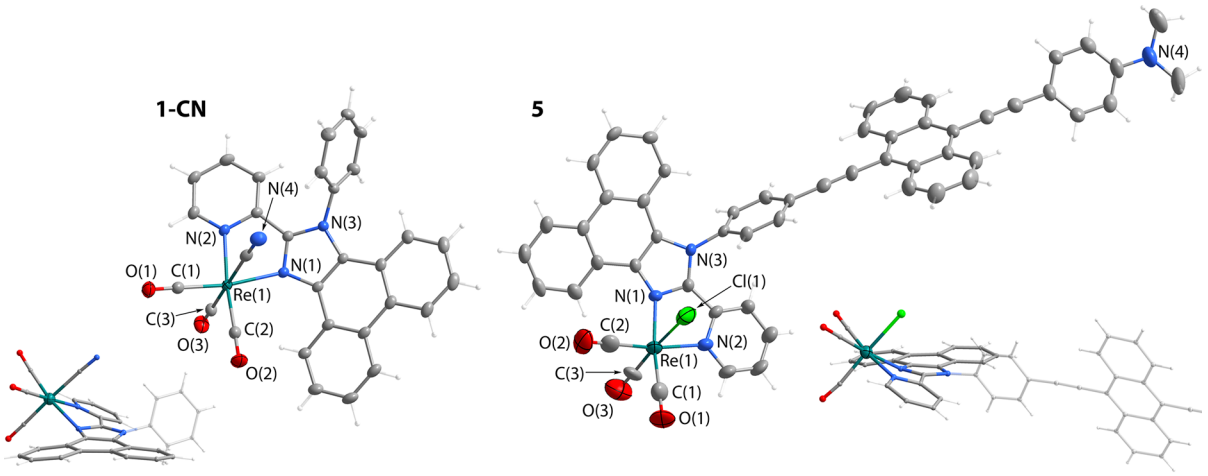

Figure 3. Molecular views of complexes **1-CN** and **5** (thermal ellipsoids are shown at the 50% probability level).

anthracenyl (an) chromophores), the electronic properties of which define their optical behavior and therefore substantially differentiate **L1**/**L2**, **L3**, and **L4**/**L5**. The UV−vis spectra for **L1** and **L2** in dichloromethane solution are very much alike and display absorption bands in the range 250−360 nm (Table 1

Table 1. Experimental and Calculated Electronic Absorption Data for L1 and L3−L5

	exptl		calcd		
	λ, nm	ε, M^{-1} cm^{-1}	λ, nm	f	MO configuration, % contribution
L1	362	13000	343	0.76	HOMO → LUMO, 94
	330	17000	319	0.04	HOMO → L+1, 83
	261	58000	284	0.09	H-1 → LUMO, 37; HOMO → L+2, 30
L3	425	20000	447	0.62	HOMO → LUMO, 99
	402	22000			
	362	20000	343	0.75	H-1 → L+1, 95
L4	464	12000	529	0.44	HOMO → LUMO, 94
	409	1200	431	0.32	H-2 → LUMO, 94
	363	26000	343	0.73	H-1 → L+1, 95
L5	490	52000	561	1.44	HOMO → LUMO, 99
	363	20000	355	0.25	HOMO → L+2, 91

and Figure S9), corresponding to the $\pi-\pi^*_{phen}$ transitions in the aromatic systems, whereas in the case of **L3** the presence of the anthracene moiety results in the appearance of additional longer wavelength absorptions (380−430 nm). Ligands **L4** and **L5**, functionalized with electron-donating $-NR_2$ groups, expectedly display broad bathochromically shifted bands (470 and 490 nm) attributed to the intramolecular charge transfer.

According to TD-DFT calculations (using PBE0 hybrid density functional taking into account dichloromethane solvent with the C-PCM method), the predicted lowest energy excitations $S_0 \rightarrow S_1$ for **L1** and **L3**−**L5** are mainly HOMO → LUMO in character (Table 1). For **L1**, it involves phenanthrene-localized $\pi \rightarrow \pi^*_{phen}$ transition mixed with phenanthrene → pyridyl charge transfer, LC/ILCT (Figure 4). In **L3** both the HOMO and LUMO are located on the ethynyl-anthracene fragment with some participation of the phenylene spacer (Figure S10). For **L4** and **L5** the HOMO is substantially delocalized over the entire anthracene-containing chromophore (Figure 4 and Figure S10), which leads to a

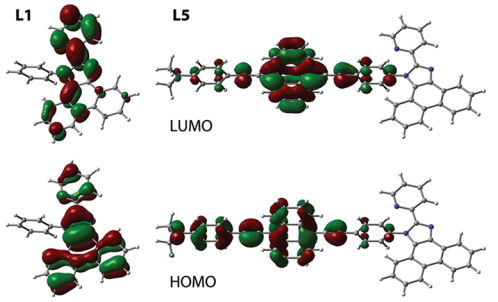

Figure 4. Frontier molecular orbitals for **L1** and **L5**.

visible charge transfer (ILCT) as a result of the $S_0 \rightarrow S_1$ transition. Computationally assessed absorptions (Table 1) correlate rather well with experimental data for **L1** and **L3**, which feature $\pi\pi^*$ character of transitions. However, for CT compounds **L4** and **L5** the energies of $S_0 \rightarrow S_1$ transitions are considerably underestimated.

Compounds **L1** and **L2** exhibit nearly identical violet-blue photoluminescence in solution (Figure 5 and Table 2), which is

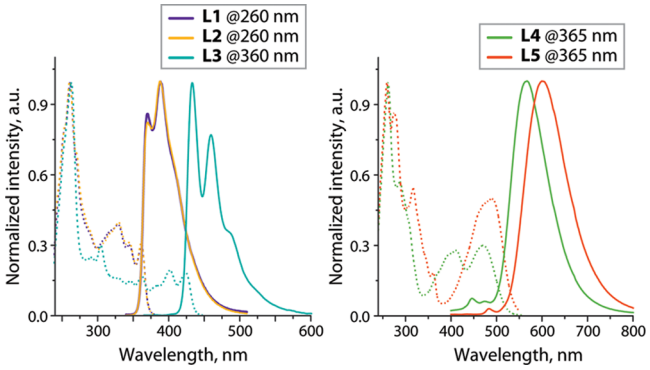

Figure 5. Normalized excitation (dotted lines) and emission (solid lines) spectra of **L1**−**L5** (CH_2Cl_2, 298 K).

insensitive to molecular oxygen ($^3O_2$) and has a short lifetime of 1.9 ns that indicates its singlet origin. The emission bands are vibronically structured (ν ca. 1250 cm^{-1}), showing no effect of the bromide substituent in **L2**, which is in accordance with the $^1\pi\pi^*_{phen}$ nature of the excited state, dominated by the orbitals of the phenanthroimidazole system. Both the absorption and

DOI: 10.1021/acs.inorgchem.8b00422
Inorg. Chem. 2018, 57, 6349−6361

Table 2. Emission Spectral Data for L1−L5 (298 K, Aerated CH_2Cl_2)

	λ_{em}, nm[a]	Φ, %[a]	τ, ns	k_r, s^{-1} [b]	k_{nr}, s^{-1} [c]
L1	370, 388	37	1.9 ± 0.1	1.9×10^8	3.3×10^8
L2	370, 388	22	1.9 ± 0.1	1.2×10^8	4.1×10^8
L3	433, 459, 486	65	3.3 ± 0.2	2.0×10^8	1.1×10^8
L4	446w, 475w, 566	52	2.1 ± 0.1 (446 nm); 1.4 ± 0.1 (566 nm)	3.7×10^8	3.4×10^8
L5	484w, 602	92	2.6 ± 0.1 (484 nm); 3.8 ± 0.2 (602 nm)	2.4×10^8	2.1×10^7

[a] λ_{ex} 260 nm (**L2**, **L3**), 360 nm (**L3**), 365 nm (**L4**, **L5**). [b] k_r values were estimated by Φ/τ_{obs}. [c] k_{nr} values were estimated by $(1 - \Phi)/\tau_{obs}$.

fluorescence spectra of **L1** and **L2** are very similar to those of 1,2-diphenyl-1*H*-phenanthro[9,10-*d*]imidazole and the derivatives,[69,70] which supports the given assignment.

The emission band of **L3** is substantially red shifted and looks essentially the same as the fluorescence profiles of phenylenthynyl-anthracene and the related anthracene-based compounds.[71,72] This observation correlates with the results of a theoretical analysis (Figure S10), which points to a major contribution of the anthracene moiety into the lowest-lying S_1 state of $\pi\pi^*_{an}$ nature. Notably, the congener dye bearing an anthracenyl unit at the N1-phenylene spacer of diphenylphenanthroimidazole[73] shows a different electronic structure with the HOMO and LUMO distributed over the phenanthrene and anthracene fragments, respectively.

Ligands **L4** and **L5** display emissions with observed lifetimes of several nanoseconds and intensities being insensitive to the presence of molecular oxygen that corresponds to prompt fluorescence. In contrast to **L1**−**L3**, compounds **L4** and **L5** containing pendant amine groups display structureless emission bands of considerably lower energy (Table 2 and Figure 5). These variations in luminescence characteristics indicate crucial changes in the character of the electronic transitions, which are associated with ILCT arising from the donor−acceptor (R_2N−π-imidazole) molecular structure of **L4** and **L5** (Figure 4 and Figure S10). Consequently, these dyes show strong fluorescence solvatochromism (Table 3, Figure 6, and Figure S11). Increasing polarity of the solvent (cyclohexane < toluene < dichloromethane < dimethylformamide) results in the bathochromic shift of the major emission band maximum to 2845 cm^{-1} (**L4**) and 4853 cm^{-1} (**L5**). The lowest energy absorptions are visibly less influenced by the variation of the solvent, which corresponds to the trends typical for charge-transfer luminophores.[74,75] For both fluorophores the highest emission intensity was determined in dichloromethane solutions, with quantum yields Φ_{em} reaching 52% and 92% for **L4** and **L5**, respectively. The optical and electronic properties of **L5** are close to those of the Me_2N−C_6H_4−C_2−anthracenyl−C_2−C_6H_4−X chromophore (X = electron-withdrawing group),[76,77] confirming a negligible participation of phenanthroimidazole in the observed electronic transitions for **L5**. A severe drop in Φ_{em} for **L5** in a polar solvent (DMF, Φ_{em} = 7%) is comparable to that observed for this bipolar diethynylanthracene congener[76] and is in line with a larger Stokes shift that implies more explicit geometry distortions of the S_1 state and, consequently, more efficient nonradiative relaxation processes.

The emission energies of **L4** and **L5** show a linear dependence of the medium dielectric constant, which can be conventionally varied by using mixtures of two different solvents (e.g., toluene/CH_2Cl_2, Figure 6 and Figure S11). This type of dependence is common for systems with photoinduced ILCT where stabilization of charge separated (i.e., polarized) excited state by means of dipole (solute)−dipole (solvent) interactions accounts for the red shift of emission in a polar environment.[34,74,76,78] A Lippert−Mataga analysis reveals satisfactory linear correlation of the Stokes shift with the solvent polarity (see Figure S12 and the accompanying calculations), from which differences in the electric dipole moment between the S_0 and S_1 states ($\Delta\mu$) for **L4** and **L5** were found to be 29 ± 5 and 44 ± 8 D, respectively. These values correlate well with those obtained for donor−acceptor species with comparable linear dimensions.[75,78]

In addition to the main low-energy ILCT emission band, it is possible to distinguish weak high energy signals in the spectra of **L4** and **L5** (measured from multiply recrystallized samples to exclude the impurities), which are most clearly seen in DMF solutions (Figure 6 and Figures S11 and S13). It should be noted that the increase in HE/LE intensity ratio for **L5** in DMF is primarily ascribed to the decrease in LE charge-transfer emission. The difference in the excitation spectra, monitored at the HE and LE bands (Figure S13), suggests two independent emissive states, which are not exceptional for donor−acceptor compounds.[78−80] The structured profile of the HE emissions may be ascribed to anthracene-centered $\pi\pi^*$ transitions, which lack charge-transfer character. The corresponding excitation patterns for HE bands (Figure S13) are reminiscent of those for **L3** and the related compounds[72] and reveal a red shift typically found for diethynyl anthracene derivatives in comparison to the monosubstituted species. In accordance with the suggested assignment, the energies of HE bands demonstrate insignificant solvatochromic dependence due to an expectedly smaller change in the dipole moment upon $\pi\pi^*$ excitation.

Table 3. Photophysical Data for L4 and L5 in Different Solvents

	solvent	λ_{abs}, nm (ε, 10^4 M^{-1} cm^{-1})	λ_{em}, nm	Φ, %[b]	τ, ns (aer)
L4	cyclohexane	260 (11.2), 310 (3.6), 344 (2.6), 363 (2.6), 409 (0.8), 472 (0.9)	440w, 503	41	c
	toluene	314 (5.9), 345 (4.3), 364 (3.9), 409 (1.2), 470 (1.3)	443w, 531	47	1.4 (443 nm); 8.7 (531 nm)
	CH_2Cl_2	262 (13.5), 311 (5.6), 344 (3.6), 363 (2.6), 409 (1.2), 464 (1.2)	446w, 475w, 566	52	2.1 (446 nm); 1.4 (566 nm)
	DMF	312 (6.4), 343 (3.8), 362 (2.9), 411 (1.4), 465 (1.4)	444w, 472w, 587	38	3.9 (444 nm); 1.4 (587 nm)
L5	cyclohexane[a]	261 (17), 268 (15), 316 (6), 344 (3), 363 (3), 459 (5)	509, 542	64	c
	toluene	319 (5.8), 364 (2.7), 471 (4.9), 490 (4.9)	539	77	2.5 (539 nm)
	CH_2Cl_2	261 (12.4), 273 (9.8), 318 (5.9), 363 (2.0), 471 (4.9), 490 (5.2)	484w, 602	92	2.6 (484 nm); 3.8 (602 nm)
	DMF	319 (6.0), 362 (2.0), 473 (4.6), 495 (5.3)	484mw, 518w, 676	7	2.8 (484 nm); 3.2 (671 nm)

[a] Extinction coefficients in cyclohexane are estimated approximately due to low solubility of **L5**. [b] λ_{ex} 365 nm. [c] Could not be determined accurately due to low solubility.

DOI: 10.1021/acs.inorgchem.8b00422
Inorg. Chem. 2018, 57, 6349−6361

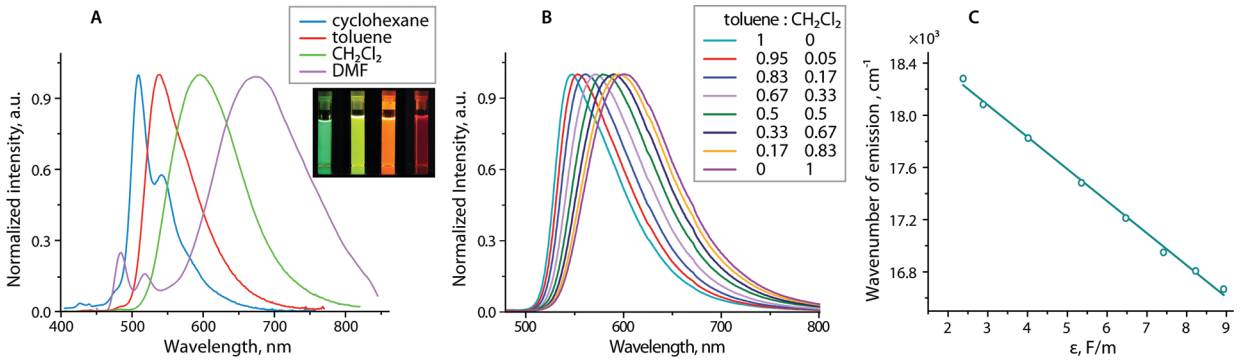

Figure 6. Normalized emission spectra of **L5** at 298 K: (A) in various solvents, with the inset showing their visual appearance under UV light (λ 365 nm); (B) in toluene−CH_2Cl_2 mixtures; (C) dependence of the emission energy on polarity (dielectric constant) of toluene−CH_2Cl_2 solutions, R^2 = 0.996.

Response to Protonation. The electron-donating N-functions of **L1**−**L5** can be easily protonated, which substantially affects the photophysical characteristics of these compounds. Adding an excess of trifluoroacetic acid to solutions of **L1** and **L2** causes an immediate appearance of a yellow-greenish color and changes the emission from deep blue (λ_{em} 370, 388 nm) to vivid green due to the emergence of two broad bands maximized at ca. 413 and 517 nm (Figure 7 and Figure S14).

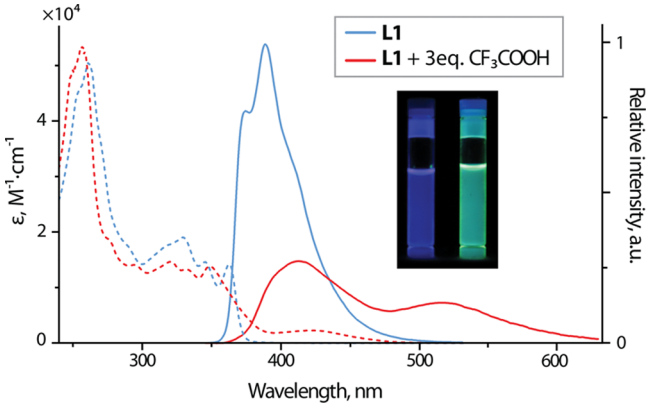

Figure 7. Effect of protonation on the absorption and emission spectra of **L1** ($c = 5.8 \times 10^{-5}$ M, CH_2Cl_2, 298 K). The inset shows the visual appearance of **L1** (left) and $[\mathbf{L1} + H]^+$ (right) under UV light (λ 365 nm).

The corresponding ^{1}H NMR spectra (Figure S15) indicate that protonation most probably occurs on the diimine (pyridyl-imidazole) part of the molecule, which is reflected by the large low-field shift of the pyridyl H(9) atom as a result of electronic deshielding, analogously to the coordination-induced shift observed for rhenium complexes (Figure S8). Protonation of the pyridinium fragment is expected to stabilize the LUMO level that activates the $ILCT_{phen\rightarrow py}$ excited state and decreases the energies of both absorption and emission. Reminiscent variations in the optical characteristics due to an emission switch to the ILCT mode have been recently described for a phenanthro-imidazole probe for formaldehyde.[81] Treatment of **L3** and **L4** with the acid leads to a large decrease in fluorescence intensity without a considerable change in emission energy (Figure S14). This effect might be attributed to the increased electron-withdrawing ability of the diimine motif that facilitates photoinduced electron transfer from the anthracene-based donor. The basicity of the terminal $Ph_2N-C_6H_4-$ group in **L4** is expected to be much lower than that of pyridyl and dimethylaminophenyl functions (in **L5**) (pK_a values of conjugate acids of pyridine, dimethylaniline, and Ph_3N in acetonitrile are 12.53, 11.43, and 1.3, respectively[82,83]); therefore, protonation of the diphenylamine group in **L4** is not likely to occur.

In the case of **L5**, however, the high proton affinity of the aniline $Me_2N-C_6H_4-$ function is evidently responsible for reversible switching of the optical properties. In acidic medium the long-wavelength absorption (492 nm) is gradually decreased, which is accompanied by the simultaneous growth of the adjacent blue-shifted band with a clearly distinguishable isosbestic point at 476 nm (Figure 8). Accordingly, the low-

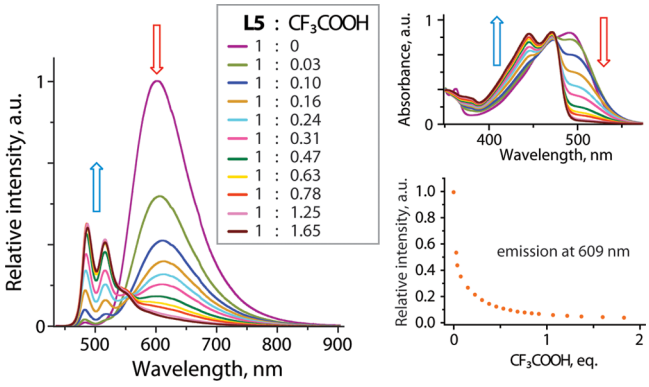

Figure 8. Effect of protonation on the absorption and emission spectra of **L5** ($c = 10^{-5}$ M, CH_2Cl_2, 298 K).

energy broad charge-transfer emission (602 nm in CH_2Cl_2) is replaced by the high-energy structured band (487 nm) that is assigned to $\pi \rightarrow \pi^*_{an}$ anthracene-centered transitions. Addition of a base (e.g., triethylamine, DBU) restores the original orange ILCT fluorescence.

Rhenium(I) Complexes. The photophysical properties of compounds **1**−**5** and **1-CN** are summarized in Table 4. The absorption spectra of **1**, **1-CN**, and **2** in dichloromethane solution (Figure S16) display high-energy (HE) bands at ca. 260 nm, which are primarily assigned to $^1\pi \rightarrow \pi^*_{phen}$ transitions within the aromatic system of the phenanthro-diimine fragments. The longer wavelength weaker absorptions with maxima at ca. 375−378 nm ($\varepsilon = (2.1-2.3) \times 10^4$ M^{-1} cm^{-1}) and tails up to 450 nm are not observed for the free ligands and apparently correspond to the spin-allowed ^{1}ML′LCT (L′ = Cl/

DOI: 10.1021/acs.inorgchem.8b00422
Inorg. Chem. 2018, 57, 6349−6361

Table 4. Photophysical Properties of Complexes 1−5 and 1-CN in Solution (Degassed CH_2Cl_2, 298 K)

	λ_{abs}, nm (ε, 10^4 M^{-1} cm^{-1})	λ_{em}, nm	Φ, %[a]	τ_{obs}, ns	k_r, s^{-1} [b]	k_{nr}, s^{-1} [c]
1	259 (5.1), 377 (2.1)	369, 392, 408, 616	2 (616 nm)	2.6 ± 0.1 (392 nm); 186 ± 9 (616 nm)	1.1×10^5	5.3×10^6
1-CN	258 (5.8), 375 (2.2)	582	20	3550 ± 250	5.6×10^4	2.3×10^5
2	259 (6.1), 378 (2.3)	371, 392, 407, 624	2 (624 nm)	2.1 ± 0.1 (405 nm); 142 ± 7 (624 nm)	1.4×10^5	6.9×10^6
3	263 (14.1), 303 (2.9), 384 (3.4), 403 (3.4), 427 (2.5)	436, 460, 486(sh)	3	4.1 ± 0.2	7.3×10^6	2.4×10^8
4	262 (18.8), 384 (4.9), 470 (2.1)	572	10	4.5 ± 0.2	2.2×10^7	2.0×10^8
5	260 (15.2), 380 (3.9), 478 (6.5), 493 (6.4)	614	22	2.7 ± 0.1	8.1×10^7	2.9×10^8

[a] λ_{ex} 365 nm. [b] k_r values were estimated by Φ/τ_{obs}. [c] k_{nr} values were estimated by $(1 - \Phi)/\tau_{obs}$.

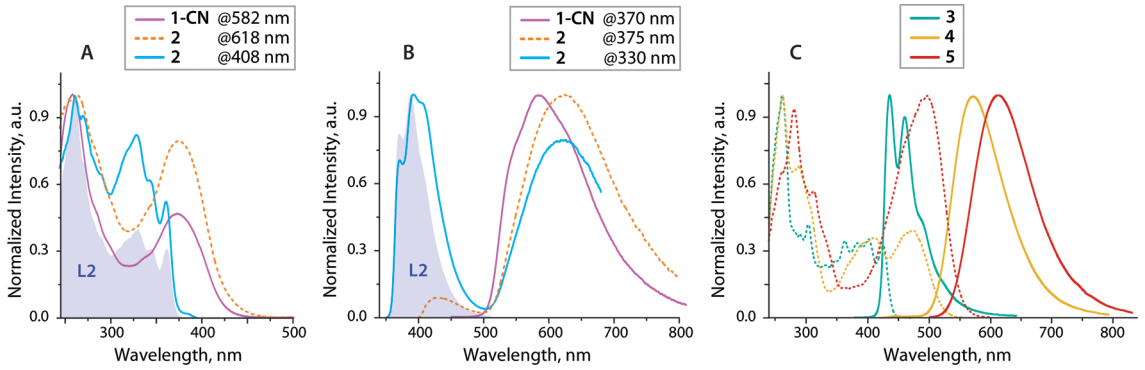

Figure 9. Normalized excitation (A) and emission (B) spectra of **1-CN** and **2** (the corresponding spectra of **L2** (filled) are shown for comparison) and (C) excitation (dotted lines) and emission spectra (solid lines) of **3−5** (degassed CH_2Cl_2, 298 K).

CN/CO) transitions (i.e., $\{Re(CO)_3X\}$ → NN ligand, Figure S17 and Table S3), which conforms with earlier theoretical and spectroscopic investigations of $[Re(CO)_3X(diimine)]$ compounds.[84−88]

The UV−vis absorption patterns of **3−5** are reminiscent of those obtained for free ligands **L3−L5**. In the low-energy region these complexes feature electronic transitions, which are determined by the anthracene-based chromophores (Figure S18 and Table S3). These bands are only slightly red shifted with respect to those of **L3−L5**, which contrasts with the coordination response of donor-functionalized dipyridophenazine[34,78] and pyridyl-triazole[19] ligands and points to essentially independent electronic behavior of phenathro-diimine and anthracene motifs. Nevertheless, the ILCT absorptions for **4** and **5** demonstrate a substantial increase in extinction coefficients to 21000 and 64000 $M^{-1}{\cdot}cm^{-1}$, respectively (cf. 12000 and 52000 $M^{-1}{\cdot}cm^{-1}$ for **L4** and **L5**). Analogously to the aforementioned compounds **1** and **2**, the ML′LCT band at ca. 380 nm is evidently present for **3−5** as well and is clearly visible in the spectrum of **5** (but is absent for **L5**; Figure S16).

Complexes **1−5** and **1-CN** are luminescent at room temperature both in solution and in the solid state (except **3**) (see Figure 9 and Figures S19 and S20). In fluid medium **1** and **2** demonstrate dual emission, which is possible to manipulate by varying the excitation wavelength. Selective irradiation into the long-wavelength absorption (λ_{exc} 375 nm) of **1** and **2** results in a predominantly low-energy structureless emission with a maximum at ca. 620 nm (Φ_{em} = 2%) and lifetimes of 0.19 (**1**)/0.14 (**2**) μs (Table 4); the latter values are comparable to those of other Re(I) diimine tricarbonyl compounds.[37,38,67,89,90] The intensity of the LE band appreciably decreases in aerated solution, which suggests a triplet origin of the excited state (i.e., ^{3}ML′LCT likely mixed with some ^{3}LC). Higher energy excitation (λ_{exc} 330 nm) results in appearance of an HE band with a maximum at 392 nm, particularly pronounced for complex **2** (Figure 9B), in addition to low-energy ^{3}CT emission. The vibronic structure (ν ca. 1440 cm^{-1}) of the HE band, its position, and the corresponding excitation spectrum, which are close to those of **L1** and **L2**, point to the ligand-centered ^{1}LC nature of HE emissions (i.e., fluorescence) that is also evidenced by short lifetimes of 2.1−2.6 ns.

In this respect it should be noted that Re(I) diimine complexes, dually emissive in solution under ambient conditions, are rare. Thus, two ^{3}MLCT emissive states with nearly the same energies arising from different conformers were proposed for $[Re(Me_2bipy)(CO)_2(PR_3)_2]^+$ compounds.[91] Two clearly resolved emission bands assigned to $^1\pi\pi^*$ (HE) and $^3\pi\pi^*$ (LE) origins were observed for the family of $[Re(NN)(CO)_3Cl]$ species (NN = pyridylimidazo[1,5-*a*]pyridine ligands), though at a low intensity of less than 0.3%.[92,93] Ultimately, dual luminescence from $\pi\pi^*$ (HE) and MLCT (LE) levels was suggested for dirhenium metallacycle[94] and $[Re(NN)(CO)_3Cl]$ compounds (NN = dipyridophenazine-based ligands),[95] while for $[Re(NN)(CO)_3(L)]^{+/0}$ species both ^{1}ILCT and ^{3}MLCT excited states were found to undergo radiative relaxation in solution.[44] In addition, a few complexes bearing pendant fluorophores exhibit singlet and triplet luminescence from two different spatially separated emissive centers.[39,43,96]

The unconventional behavior of **1** and **2** can be tentatively rationalized by the qualitative energy level diagram (Figure 10). It is assumed that, due to the presence of a polyaromatic phenanthrene system, irradiation of these complexes with λ_{exc} 330 nm can optically populate both ligand-centered $^1\pi\pi^*_{phen}$ and ^{1}ML′LCT states, which are normally not mixed due to the large energy separation[87] and thus can potentially relax following independent pathways. The singlet charge-transfer

DOI: 10.1021/acs.inorgchem.8b00422
Inorg. Chem. 2018, 57, 6349−6361

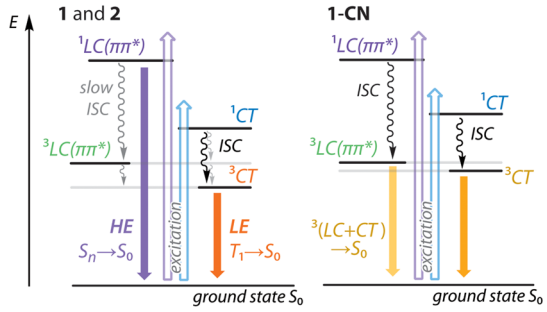

Figure 10. Qualitative energy level diagram for **1** and **2** (left) and **1-CN** (right).

state expectedly undergoes fast intersystem crossing (ISC) to the lowest triplet ^{3}CT state, responsible for the long-lived phosphorescence signal at ca. 620 nm. This assignment in general matches the excited ^{1}CT state dynamics of [Re(CO)$_3$X(bipy)] compounds in detail studied by ultrafast spectroscopy and theoretical studies involving spin−orbit coupling calculations.[97,98]

However, for the $^1\pi\pi^*_{phen}$ state the ISC process seems to be too slow to completely overcome prompt radiative relaxation $S_n \rightarrow S_0$ that generates a fluorescence band maximized at 392 nm. Slow rates of ISC for ^{1}LC excited states have been claimed for some other second- and third-row metal complexes with the ligand emissive centers directly bound to the metal ions.[16,99−101] In the case of the proposed ^{1}LC($\pi\pi^*$) state the ISC is symmetry forbidden (due to the same origin of molecular orbitals involved in $^1\pi\pi^*$ and $^3\pi\pi^*$ states)[102] and might become allowed by mixing with higher energy MLCT states.[101] Changing the chloride for cyanide in **1** has a dramatic influence on the photophysical performance. The emission of **1-CN** is independent of the excitation energy and reveals a poorly structured profile (Figure 9B). Together with a nearly 20-fold increase in lifetime (from 0.19 to 3.55 μs) and a visible hypsochromic shift of 948 cm^{-1} (34 nm) in comparison with **1**, these results point out that the emissive excited state changed its character and now consists of ^{3}ML′LCT and ^{3}LC contributions. Despite the fact that the radiative rate constant for **1-CN** is two times smaller than that for **1** (k_r = 5.6 × 10^4 and 1.1 × 10^5 s^{-1}, respectively), which also complies with the somewhat different lowest lying triplet state, the cyanide derivative shows a 1 order of magnitude higher quantum efficiency (Φ_{em} = 20%) due to largely suppressed nonradiative relaxation processes. It is known that the ancillary X ligand in [Re(CO)$_3$X(NN)] compounds (X = pseudohalide or neutral L) can strongly affect the ^{3}MLCT/^{3}ML′LCT levels.[31,35,103] For the complexes with small energy separation between the ML′LCT and LC triplet states the variation in X nature (e.g., substitution of Cl for pyridine)[35] or its electronic characteristics (protonation or boronation of −CN)[90,104] can rise the energy of a triplet charge transfer level so that it becomes comparable to or exceeds that of the ^{3}LC transition. Furthermore, a better π-accepting ability of CN$^-$ vs Cl$^-$ simultaneously to increasing the energy of the ^{3}ML′LCT state is expected to stabilize the ground state of **1-CN**, causing a hypsochromic shift in emission and a decrease in radiative rate constant. The absence of a HE fluorescence band in the spectrum of **1-CN** under 330 nm excitation shows that the ISC ($^1\pi\pi^* \rightarrow {}^3\pi\pi^*$) rate is faster than $S_n \rightarrow S_0$ decay. However, the proposed largely oversimplified model does not allow us to rationalize the hypothesized facilitation of intradiimine ISC upon substitution of Cl for CN. One plausible explanation might originate from increased energies of higher ML′LCT excited states in **1-CN** that could lead to their more effective mixing with the ^{1}LC state.[101] Furthermore, it has been shown computationally that Re−X stretching modes (which are eventually different for **1** and **1-CN**) can participate in vibronic coupling of the spin-mixed CT excited states[105−107] and therefore may also influence these second-order LC−ML′LCT interactions.

In the solid state complexes **1**, **1-CN**, and **2** behave very much alike (Figure S20 and Table S4) and display vibronically structured luminescence bands. The values of observed lifetimes (3.9−4.7 μs) are close to that determined for **1-CN** in solution, which indicates a certain similarity of their emissive excited states (i.e., significant mixing of ^{3}CT and ^{3}LC characters). Destabilization of the ^{3}CT state due to a phase transition (solution → solid) that accounts for a change in the lowest lying excited state (or efficient ^{3}IL−^{3}CT coupling) for **1** and **2** is not uncommon for Re(I) phosphors[87,90] and confirms the small energy gap $\Delta E(^3\text{IL}-{}^3\text{CT})$ suggested above.

The character of luminescence in **3**−**5** is different, as no MLCT contribution was observed regardless of the excitation wavelength; only the short-lived singlet emission associated with the anthracene-based moiety has been detected (Figure 9C and Table 4). For all of these complexes the excitation and emission profiles virtually coincide with the corresponding spectra of the parent ligands **L3**−**L5**. A small red shift (159−325 cm^{-1}) of the emission maxima in **3**−**5** means that coordination of the metal center introduces only a slight perturbation to the frontier molecular orbitals. Completely in line with the behavior of uncoordinated organic compounds with ILCT features (**L4** and **L5**) the emissions of the corresponding complexes **4** and **5** display strong dependence on the nature of solvents, media polarity, and the presence of the protonating agent (Figure S21 and Table S5). Furthermore, the ligand-originated fluorescence correlates with the results of theoretical analysis, according to which the lowest lying excited state S_1 for **3**−**5** is delocalized over the ancillary chromophore (Table S3 and Figure S18).

Quantum yields for **3**−**5** are appreciably lower with respect to those of the parent ligands **L3**−**L5**, which is reflected by much smaller radiative rate constants calculated for the metal complexes. Gradually decreasing the energy of the ligand-based lowest lying excited state (^{1}ILCT) results in less drastic emission quenching (Φ_{em} = 10% and 22% for **4** and **5**). The lifetimes for **3**−**5** (τ_{obs} = 4.1, 4.5, 2.7 ns) are on the same order as those of the ligands (3.3, 1.4, and 3.8 ns for **L3**−**L5**) meaning that the drop in fluorescence intensity upon complexation is not determined by the energy transfer from organic chromophores to the metal ion and other components of the coordination sphere.

Interestingly, the excitation spectrum of **5** does not reveal an MLCT band around 380 nm, which is resolved in the absorption spectrum. This points to the lack of MLCT participation in the dynamic processes which lead to the emissive excited state, indicating no appreciable energy transfer ^{1}MLCT → ^{1}ILCT occurs. Efficient nonradiative relaxation of the ^{3}MLCT state in Re compounds containing the anthracene motif has been previously rationalized by sensitization of the polyaromatic triplet state (i.e., ^{3}MLCT → $^3\pi\pi^*_{an}$).[40,108] In the case of **4** and **5** a similar triplet−triplet energy transfer (^{3}MLCT → ^{3}ILCT) also seems to be a feasible pathway to quench the emission from the {Re(diimine)} fragment. An alternative possibility that cannot be ruled out on the basis of the available

DOI: 10.1021/acs.inorgchem.8b00422
Inorg. Chem. 2018, 57, 6349−6361

data involves electron transfer from the electron-rich chromophore to the photoexcited {Re^{II}(diimine)} motif; such a process is not exceptional for rhenium(I) luminophores, and its probability depends on the properties of the diimine ligand.[43,108] The described photophysical behavior of **4** and **5** clearly contrasts with optical characteristics of the majority of rhenium(I) diimine compounds, which predominantly exhibit triplet emission or the formation of the intraligand dark triplet states.[32−36]

CONCLUSIONS

We have developed the family of readily accessible diimine ligands based on a coordinating pyridyl-phenanthroimidazole motif (**L1**, **L2**), which was functionalized with electron-rich anthracene-based units to give bichromophoric molecules **L3**−**L5**. The optical properties of ligands **L1** and **L2** are defined by $\pi\pi^*$/CT (phenanthrene → pyridyl) electronic transitions, whereas for **L3**−**L5** they are localized in the anthracene motif. The donor−acceptor architecture of **L4** and **L5** enables efficient low-energy intramolecular charge-transfer transitions (maximum λ_{abs} 490 nm with tails below 550 nm for **L5** in CH_2Cl_2). The title compounds are luminescent in solution, showing moderate to high quantum efficiencies, and cover a wide range of emission wavelengths from violet to orange-red (Φ_{em} = 22−92%, λ_{em} 370−602 nm in CH_2Cl_2). The charge-transfer character of emission for **L4** and **L5** determines their pronounced fluorescence solvatochromism. The presence of electron donor groups (pyridyl and dimethylaminophenyl) susceptible to protonation allows for reversible switching of emission parameters by affecting the charge-transfer processes. Ligands **L1**−**L5** easily get coordinated to the rhenium(I) center, forming the corresponding complexes of the general composition [$Re(CO)_3X$(diimine)] (X = Cl, **1**−**5**; X = CN, **1-CN**). Compounds **1** and **2** demonstrate dual fluorescence−phosphorescence arising from the same organic fragment that is a rare behavior for rhenium(I) luminophores. This phenomenon is tentatively attributed to the excitation-dependent population of poorly coupled $^1\pi\pi^*$ and ^{3}CT excited states, which undergo independent radiative relaxation leading to high- and low-energy emission bands. Changing the chloride for cyanide has a pronounced effect on luminescence intensity that reveals 10-fold increase in **1-CN** in comparison with **1**.

Photoemission of complexes **3**−**5** is dominated by the intraligand transitions, only slightly perturbed by the presence of the metal ion. The lack of phosphorescence originating from ^{3}ML′LCT or ^{3}IL(phenanthrene) might be explained by the triplet energy transfer to the nonemissive state of the anthracene moiety. Moderately intense intraligand fluorescence detected for **4** and **5** is drastically different from the properties of the major part of the known rhenium(I) luminophores.

The reported ligands, showing intense absorption and emission bands in a wide range of the visible spectrum, are thought to be suitable for the preparation of a variety of photofunctional coordination metal complexes.

ASSOCIATED CONTENT

Supporting Information

The Supporting Information is available free of charge on the ACS Publications website at DOI: 10.1021/acs.inorgchem.8b00422.

Preparation of the ligands **L1**−**L5**, crystallographic and computational details, and ESI-MS, NMR, and additional photophysical data (PDF)

Accession Codes

CCDC 1824098−1824103 contain the supplementary crystallographic data for this paper. These data can be obtained free of charge via www.ccdc.cam.ac.uk/data_request/cif, or by emailing data_request@ccdc.cam.ac.uk, or by contacting The Cambridge Crystallographic Data Centre, 12 Union Road, Cambridge CB2 1EZ, UK; fax: +44 1223 336033.

AUTHOR INFORMATION

Corresponding Authors

*E-mail for S.P.T.: stunik@inbox.ru.
*E-mail for I.O.K.: igor.koshevoy@uef.fi.

ORCID

Sergey P. Tunik: 0000-0002-9431-0944
Igor O. Koshevoy: 0000-0003-4380-1302

Notes

The authors declare no competing financial interest.

ACKNOWLEDGMENTS

The authors greatly appreciate financial support from the Russian Science Foundation (grant 16-43-03003, synthesis and photophysical studies) and the Finnish National Agency for Education for a CIMO Fellowship (K.S.K., structural characterization). We acknowledge grants of computer capacity from the Finnish Grid and Cloud Infrastructure (persistent identifier urn:nbn:fi:research-infras-2016072533). The work was carried out using the core facilities of St. Petersburg State University Research Park (Centre for Magnetic Resonance, Centre for Optical and Laser Materials Research, Centre for Chemical Analysis and Materials Research, and Centre for X-ray Diffraction Studies).

REFERENCES

(1) Schwartz, E.; Le Gac, S.; Cornelissen, J. J. L. M.; Nolte, R. J. M.; Rowan, A. E. Macromolecular multi-chromophoric scaffolding. *Chem. Soc. Rev.* **2010**, *39*, 1576−1599.
(2) Farinola, G. M.; Ragni, R. Electroluminescent materials for white organic light emitting diodes. *Chem. Soc. Rev.* **2011**, *40*, 3467−3482.
(3) Marszalek, T.; Li, M.; Pisula, W. Design directed self-assembly of donor−acceptor polymers. *Chem. Commun.* **2016**, *52*, 10938−10947.
(4) Coughlin, J. E.; Henson, Z. B.; Welch, G. C.; Bazan, G. C. Design and Synthesis of Molecular Donors for Solution-Processed High-Efficiency Organic Solar Cells. *Acc. Chem. Res.* **2014**, *47*, 257−270.
(5) Castellano, F. N. Altering Molecular Photophysics by Merging Organic and Inorganic Chromophores. *Acc. Chem. Res.* **2015**, *48*, 828−839.
(6) Lees, A. J. Luminescence Properties of Organometallic Complexes. *Chem. Rev.* **1987**, *87*, 711−743.
(7) Xiang, H.; Zhou, L.; Feng, Y.; Cheng, J.; Wu, D.; Zhou, X. Tunable Fluorescent/Phosphorescent Platinum(II) Porphyrin−Fluorene Copolymers for Ratiometric Dual Emissive Oxygen Sensing. *Inorg. Chem.* **2012**, *51*, 5208−5212.
(8) Yoshihara, T.; Yamaguchi, Y.; Hosaka, M.; Takeuchi, T.; Tobita, S. Ratiometric Molecular Sensor for Monitoring Oxygen Levels in Living Cells. *Angew. Chem., Int. Ed.* **2012**, *51*, 4148−4151.
(9) Zhao, Q.; Zhou, X.; Cao, T.; Zhang, K. Y.; Yang, L.; Liu, S.; Liang, H.; Yang, H.; Li, F.; Huang, W. Fluorescent/Phosphorescent Dual-Emissive Conjugated Polymer Dots for Hypoxia Bioimaging. *Chem. Sci.* **2015**, *6*, 1825−1831.
(10) Hara, D.; Komatsu, H.; Son, A.; Nishimoto, S.-i.; Tanabe, K. Water-Soluble Phosphorescent Ruthenium Complex with a Fluo-

DOI: 10.1021/acs.inorgchem.8b00422
Inorg. Chem. 2018, 57, 6349−6361

rescent Coumarin Unit for Ratiometric Sensing of Oxygen Levels in Living Cells. *Bioconjugate Chem.* **2015**, *26*, 645−649.
(11) Zhang, Y.; Jiang, H.; Liu, Y.; Zhou, K.; Wang, Y.; Tan, H.; Su, S.; Zhu, W. Dinuclear cyclometalated platinum(II) complexes containing a deep blue fluorescence chromophore: synthesis, photophysics and application in single dopant white PLEDs. *Dalton Trans.* **2016**, *45*, 14131−14140.
(12) Kozhevnikov, D. N.; Kozhevnikov, V. N.; Shafikov, M. Z.; Prokhorov, A. M.; Bruce, D. W.; Williams, J. A. G. Phosphorescence vs Fluorescence in Cyclometalated Platinum(II) and Iridium(III) Complexes of (Oligo)thienylpyridines. *Inorg. Chem.* **2011**, *50*, 3804−3815.
(13) Lu, W.; Kwok, W.-M.; Ma, C.; Chan, C. T.-L.; Zhu, M.-X.; Che, C.-M. Organic Triplet Excited States of Gold(I) Complexes with Oligo(o- or m-phenyleneethynylene) Ligands: Conjunction of Steady-State and Time-Resolved Spectroscopic Studies on Exciton Delocalization and Emission Pathways. *J. Am. Chem. Soc.* **2011**, *133*, 14120−14135.
(14) Gupta, S. K.; Haridas, A.; Choudhury, J. Remote Terpyridine Integrated NHC−IrIII Luminophores as Potential Dual-Emissive Ratiometric O2 Probes. *Chem. - Eur. J.* **2017**, *23*, 4770−4773.
(15) Bachmann, M.; Blacque, O.; Venkatesan, K. Harnessing White-Light Luminescence via Tunable Singlet-and Triplet-Derived Emissions Based on Gold(III) Complexes. *Chem. - Eur. J.* **2017**, *23*, 9451−9456.
(16) Chia, Y. Y.; Tay, M. G. An insight into fluorescent transition metal complexes. *Dalton Trans.* **2014**, *43*, 13159−13168.
(17) Zhou, X.; Tyson, D. S.; Castellano, F. N. First Generation Light-Harvesting Dendrimers with a $[Ru(bpy)_3]^{2+}$ Core and Aryl Ether Ligands Functionalized with Coumarin 450. *Angew. Chem., Int. Ed.* **2000**, *39*, 4301−4305.
(18) Spaenig, F.; Olivier, J.-H.; Prusakova, V.; Retailleau, P.; Ziessel, R.; Castellano, F. N. Excited-State Properties of Heteroleptic Iridium(III) Complexes Bearing Aromatic Hydrocarbons with Extended Cores. *Inorg. Chem.* **2011**, *50*, 10859−10871.
(19) Huff, G. S.; Lo, W. K. C.; Horvath, R.; Turner, J. O.; Sun, X.-Z.; Weal, G. R.; Davidson, H. J.; Kennedy, A. D. W.; McAdam, C. J.; Crowley, J. D.; George, M. W.; Gordon, K. C. Excited States of Triphenylamine-Substituted 2-Pyridyl-1,2,3-triazole Complexes. *Inorg. Chem.* **2016**, *55*, 12238−12253.
(20) Roussakis, E.; Spencer, J. A.; Lin, C. P.; Vinogradov, S. A. Two-Photon Antenna-Core Oxygen Probe with Enhanced Performance. *Anal. Chem.* **2014**, *86*, 5937−5945.
(21) Jiang, X.; Peng, J.; Wang, J.; Guo, X.; Zhao, D.; Ma, Y. Iridium-Based High-Sensitivity Oxygen Sensors and Photosensitizers with Ultralong Triplet Lifetimes. *ACS Appl. Mater. Interfaces* **2016**, *8*, 3591−3600.
(22) McCusker, C. E.; Hablot, D.; Ziessel, R.; Castellano, F. N. Metal Coordination Induced π-Extension and Triplet State Production in Diketopyrrolopyrrole Chromophores. *Inorg. Chem.* **2012**, *51*, 7957−7959.
(23) Zhao, J.; Wu, W.; Sun, J.; Guo, S. Triplet photosensitizers: from molecular design to applications. *Chem. Soc. Rev.* **2013**, *42*, 5323−5351.
(24) Palao, E.; Sola-Llano, R.; Tabero, A.; Manzano, H.; Agarrabeitia, A. R.; Villanueva, A.; López-Arbeloa, I.; Martínez-Martínez, V.; Ortiz, M. J. AcetylacetonateBODIPY-Biscyclometalated Iridium(III) Complexes: Effective Strategy towards Smarter Fluorescent Photosensitizer Agents. *Chem. - Eur. J.* **2017**, *23*, 10139−10147.
(25) Castellano, F. N.; McCusker, C. E. MLCT sensitizers in photochemical upconversion: past, present, and potential future directions. *Dalton Trans.* **2015**, *44*, 17906−17910.
(26) Guo, X.; Liu, Y.; Chen, Q.; Zhao, D.; Ma, Y. New Bichromophoric Triplet Photosensitizer Designs and Their Application in Triplet−Triplet Annihilation Upconversion. *Adv. Opt. Mater.* **2018**, *6*, 1700981.
(27) Lo, K. K.-W. Luminescent Rhenium(I) and Iridium(III) Polypyridine Complexes as Biological Probes, Imaging Reagents, and Photocytotoxic Agents. *Acc. Chem. Res.* **2015**, *48*, 2985−2995.
(28) Clede, S.; Policar, C. Metal−Carbonyl Units for Vibrational and Luminescence Imaging: Towards Multimodality. *Chem. - Eur. J.* **2015**, *21*, 942−958.
(29) Rohacova, J.; Ishitani, O. Photofunctional multinuclear rhenium(I) diimine carbonyl complexes. *Dalton Trans.* **2017**, *46*, 8899−8919.
(30) Lee, L. C.-C.; Leung, K.-K.; Lo, K. K.-W. Recent development of luminescent rhenium(I) tricarbonyl polypyridine complexes as cellular imaging reagents, anticancer drugs, and antibacterial agents. *Dalton Trans.* **2017**, *46*, 16357−16380.
(31) Kumar, A.; Sun, S.-S.; Lees, A. J. Photophysics and Photochemistry of Organometallic Rhenium Diimine Complexes. *Top. Organomet. Chem.* **2009**, *29*, 1−35.
(32) Lundin, N. J.; Walsh, P. J.; Howell, S. L.; McGarvey, J. J.; Blackman, A. G.; Gordon, K. C. Complexes of Functionalized Dipyrido[3,2-*a*:2′,3′-*c*]-phenazine: A Synthetic, Spectroscopic, Structural, and Density Functional Theory Study. *Inorg. Chem.* **2005**, *44*, 3551−3560.
(33) Fraser, M. G.; Blackman, A. G.; Irwin, G. I. S.; Easton, C. P.; Gordon, K. C. Effect of Sulfur-Based Substituents on the Electronic Properties of Re(I) dppz Complexes. *Inorg. Chem.* **2010**, *49*, 5180−5189.
(34) Larsen, C. B.; van der Salm, H.; Clark, C. A.; Elliott, A. B. S.; Fraser, M. G.; Horvath, R.; Lucas, N. T.; Sun, X.-Z.; George, M. W.; Gordon, K. C. Intraligand Charge-Transfer Excited States in Re(I) Complexes with Donor-Substituted Dipyridophenazine Ligands. *Inorg. Chem.* **2014**, *53*, 1339−1354.
(35) van der Salm, H.; Fraser, M. G.; Horvath, R.; Cameron, S. A.; Barnsley, J. E.; Sun, X.-Z.; George, M. W.; Gordon, K. C. Re(I) Complexes of Substituted dppz: A Computational and Spectroscopic Study. *Inorg. Chem.* **2014**, *53*, 3126−3140.
(36) Adams, B. S.; Shillito, G. E.; van der Salm, H.; Horvath, R.; Larsen, C. B.; Sun, X.-Z.; Lucas, N. T.; George, M. W.; Gordon, K. C. Alteration of Intraligand Donor−Acceptor Interactions Through Torsional Connectivity in Substituted Re-dppz Complexes. *Inorg. Chem.* **2017**, *56*, 12967−12977.
(37) Li, X.; Zhao, G.-W.; Hu, Y.-X.; Zhao, J.-H.; Dong, Y.; Zhou, L.; Lv, Y.-L.; Chi, H.-J.; Su, Z. Rational design and characterization of novel phosphorescent rhenium(I) complexes for extremely high-efficiency organic light-emitting diodes. *J. Mater. Chem. C* **2017**, *5*, 7629−7636.
(38) Yi, X.; Zhao, J.; Wu, W.; Huang, D.; Ji, S.; Sun, J. Rhenium(I) tricarbonyl polypyridine complexes showing strong absorption of visible light and long-lived triplet excited states as a triplet photosensitizer for triplet−triplet annihilation upconversion. *Dalton Trans.* **2012**, *41*, 8931−8940.
(39) Yarnell, J. E.; Deaton, J. C.; McCusker, C. E.; Castellano, F. N. Bidirectional "Ping-Pong" Energy Transfer and 3000-Fold Lifetime Enhancement in a Re(I) Charge Transfer Complex. *Inorg. Chem.* **2011**, *50*, 7820−7830.
(40) Shavaleev, N. M.; Bell, Z. R.; Easun, T. L.; Rutkaite, R.; Swanson, L.; Ward, M. D. Complexes of substituted derivatives of 2-(2-pyridyl)benzimidazole with Re(I), Ru(II) and Pt(II): structures, redox and luminescence properties. *Dalton Trans.* **2004**, 3678−3688.
(41) Yu, T.; Tsang, D. P.-K.; Au, V. K.-M.; Lam, W. H.; Chan, M.-Y.; Yam, V. W.-W. Deep Red to Near-Infrared Emitting Rhenium(I) Complexes: Synthesis, Characterization, Electrochemistry, Photophysics, and Electroluminescence Studies. *Chem. - Eur. J.* **2013**, *19*, 13418−13427.
(42) Wang, D.; Xu, Q.-L.; Zhang, S.; Li, H.-Y.; Wang, C.-C.; Li, T.-Y.; Jing, Y.-M.; Huang, W.; Zheng, Y.-X.; Accorsi, G. Synthesis and photoluminescence properties of rhenium(I) complexes based on 2,2′:6′,2″-terpyridine derivatives with hole-transporting units. *Dalton Trans.* **2013**, *42*, 2716−2723.
(43) Elliott, A. B. S.; Horvath, R.; Sun, X.-Z.; Gardiner, M. G.; Müllen, K.; Lucas, N. T.; George, M. W.; Gordon, K. C. Long-Lived Charge Transfer Excited States in HBC-Polypyridyl Complex Hybrids. *Inorg. Chem.* **2016**, *55*, 4710−4719.

DOI: 10.1021/acs.inorgchem.8b00422
Inorg. Chem. 2018, 57, 6349−6361

(44) Ramos, L. D.; Sampaio, R. N.; de Assis, F. F.; de Oliveira, K. T.; Homem-de-Mello, P.; Patrocinio, A. O. T.; Frin, K. P. M. Contrasting photophysical properties of rhenium(I) tricarbonyl complexes having carbazole groups attached to the polypyridine ligand. *Dalton Trans.* **2016**, *45*, 11688−11698.
(45) Klemens, T.; Czerwińska, K.; Szlapa-Kula, A.; Kula, S.; Świtlicka, A.; Kotowicz, S.; Siwy, M.; Bednarczyk, K.; Krompiec, S.; Smolarek, K.; Maćkowski, S.; Danikiewicz, W.; Schab-Balcerzak, E.; Machura, B. Synthesis, spectroscopic, electrochemical and computational studies of rhenium(I) tricarbonyl complexes based on bidentate-coordinated 2,6-di(thiazol-2-yl)pyridine derivatives. *Dalton Trans.* **2017**, *46*, 9605−9620.
(46) Mardanya, S.; Karmakar, S.; Maity, D.; Baitalik, S. Ruthenium(II) and Osmium(II) Mixed Chelates Based on Pyrenyl−Pyridylimidazole and 2,2′-Bipyridine Ligands as Efficient DNA Intercalators and Anion Sensors. *Inorg. Chem.* **2015**, *54*, 513−526.
(47) Qiu, K.; Ouyang, M.; Liu, Y.; Huang, H.; Liu, C.; Chen, Y.; Ji, L.; Chao, H. Two-photon photodynamic ablation of tumor cells by mitochondria-targeted iridium(III) complexes in aggregate states. *J. Mater. Chem. B* **2017**, *5*, 5488−5498.
(48) *APEX2-Software Suite for Crystallographic Programs*; Bruker AXS, Inc.: Madison, WI, USA, 2010.
(49) *CrysAlis Pro, 37.35*; Agilent Technologies: Yarnton, U.K., 2014.
(50) Sheldrick, G. M. *SADABS-2008/1-Bruker AXS Area Detector Scaling and Absorption Correction*; Bruker AXS: Madison, WI, USA, 2008.
(51) Sheldrick, G. M. Crystal structure refinement with SHELXL. *Acta Crystallogr., Sect. C: Struct. Chem.* **2015**, *71*, 3−8.
(52) Farrugia, L. J. WinGX and ORTEP for Windows: an Update. *J. Appl. Crystallogr.* **2012**, *45*, 849−854.
(53) Spek, A. L. PLATON SQUEEZE: a tool for the calculation of the disordered solvent contribution to the calculated structure factors. *Acta Crystallogr., Sect. C: Struct. Chem.* **2015**, *71*, 9−18.
(54) Spek, A. L. *PLATON, A Multipurpose Crystallographic Tool, 1.17*; Utrecht University: Utrecht, The Netherlands, 2013.
(55) Brouwer, A. M. Standards for photoluminescence quantum yield measurements in solution (IUPAC Technical Report). *Pure Appl. Chem.* **2011**, *83*, 2213−2228.
(56) Frisch, M. J.; Trucks, G. W.; Schlegel, H. B.; Scuseria, G. E.; Robb, M. A.; Cheeseman, J. R.; Scalmani, G.; Barone, V.; Petersson, G. A.; Nakatsuji, H.; Li, X.; Caricato, M.; Marenich, A. V.; Bloino, J.; Janesko, B. G.; Gomperts, R.; Mennucci, B.; Hratchian, H. P.; Ortiz, J. V.; Izmaylov, A. F.; Sonnenberg, J. L.; Williams-Young, D.; Ding, F.; Lipparini, F.; Egidi, F.; Goings, J.; Peng, B.; Petrone, A.; Henderson, T.; Ranasinghe, D.; Zakrzewski, V. G.; Gao, J.; Rega, N.; Zheng, G.; Liang, W.; Hada, M.; Ehara, M.; Toyota, K.; Fukuda, R.; Hasegawa, J.; Ishida, M.; Nakajima, T.; Honda, Y.; Kitao, O.; Nakai, H.; Vreven, T.; Throssell, K.; Montgomery, J. A., Jr.; Peralta, J. E.; Ogliaro, F.; Bearpark, M. J.; Heyd, J. J.; Brothers, E. N.; Kudin, K. N.; Staroverov, V. N.; Keith, T. A.; Kobayashi, R.; Normand, J.; Raghavachari, K.; Rendell, A. P.; Burant, J. C.; Iyengar, S. S.; Tomasi, J.; Cossi, M.; Millam, J. M.; Klene, M.; Adamo, C.; Cammi, R.; Ochterski, J. W.; Martin, R. L.; Morokuma, K.; Farkas, O.; Foresman, J. B.; Fox, D. J. *Gaussian 16*; Gaussian, Inc.: Wallingford, CT, 2016.
(57) Perdew, J. P.; Burke, K.; Ernzerhof, M. Generalized Gradient Approximation Made Simple. *Phys. Rev. Lett.* **1996**, *77*, 3865−3868.
(58) Adamo, C.; Barone, V. Toward reliable density functional methods without adjustable parameters: The PBE0 model. *J. Chem. Phys.* **1999**, *110*, 6158−6170.
(59) Rappoport, D.; Furche, F. Property-optimized Gaussian basis sets for molecular response calculations. *J. Chem. Phys.* **2010**, *133*, 134105.
(60) Barone, V.; Cossi, M. Quantum Calculation of Molecular Energies and Energy Gradients in Solution by a Conductor Solvent Model. *J. Phys. Chem. A* **1998**, *102*, 1995−2001.
(61) Cossi, M.; Rega, N.; Scalmani, G.; Barone, V. Energies, structures, and electronic properties of molecules in solution with the C-PCM solvation model. *J. Comput. Chem.* **2003**, *24*, 669−681.
(62) Yang, F.; Yu, T.; Zhao, Y.; Zhang, H.; Niu, Y. Synthesis, photoluminescence properties of novel cationic Ir(III) complexes with phenanthroimidazole derivative as the ancillary ligand. *Polyhedron* **2017**, *138*, 74−81.
(63) Juris, A.; Campagna, S.; Bidd, I.; Lehn, J. M.; Ziessel, R. Synthesis and photophysical and electrochemical properties of new halotricarbonyl(polypyridine)rhenium(I) complexes. *Inorg. Chem.* **1988**, *27*, 4007−4011.
(64) Moya, S. A.; Guerrero, J.; Rodriguez-Nieto, F. J.; Wolcan, E.; Féliz, M. R.; Baggio, R. F.; Garland, M. T. Influence of the 4-Substituted Pyridine Ligand L' on both the Conformation and Spectroscopic Properties of the (2,2'-Biquinoline-$\kappa N^1,\kappa N^{1'}$)-tricarbonyl(pyridine-kN1)rhenium(1+) Complex ([$Re(CO)_3$-(bqui)-(py)]+) and Its Derivatives [$Re(CO)_3$(L)(L')]+ (L= 2,2'-Biquinoline and 3,3′-(Ethane-1,2-diyl)-2,2'-biquinoline). *Helv. Chim. Acta* **2005**, *88*, 2842−2860.
(65) Wang, K.; Huang, L.; Gao, L.; Jin, L.; Huang, C. Synthesis, Crystal Structure, and Photoelectric Properties of Re(CO)3ClL (L = 2-(1-Ethylbenzimidazol-2-yl)pyridine). *Inorg. Chem.* **2002**, *41*, 3353−3358.
(66) Czerwieniec, R.; Kapturkiewicz, A.; Lipkowski, J.; Nowacki, J. Re(I)(tricarbonyl)+ complexes with the 2-(2-pyridyl)-N-methylbenzimidazole, 2-(2-pyridyl)benzoxazole and 2-(2-pyridyl)-benzothiazole ligands − syntheses, structures, electrochemical and spectroscopic studies. *Inorg. Chim. Acta* **2005**, *358*, 2701−2710.
(67) Tzeng, B.-C.; Chen, B.-S.; Chen, C.-K.; Chang, Y.-P.; Tzeng, W.-C.; Lin, T.-Y.; Lee, G.-H.; Chou, P.-T.; Fu, Y.-J.; Chang, A. H.-H. pH-Dependent Spectroscopic and Luminescent Properties, and Metal-Ion Recognition Studies of Re(I) Complexes Containing 2-(20-Pyridyl)benzimidazole and 2-(20-Pyridyl)benzimidazolate. *Inorg. Chem.* **2011**, *50*, 5379−5388.
(68) Wallace, L.; Rillema, D. P. Photophysical Properties of Rhenium(I) Tricarbonyl Complexes Containing Alkyl- and Aryl-Substituted Phenanthrolines as Ligands. *Inorg. Chem.* **1993**, *32*, 3836−3843.
(69) Yuan, Y.; Li, D.; Zhang, X.; Zhao, X.; Liu, Y.; Zhang, J.; Wang, Y. Phenanthroimidazole-derivative semiconductors as functional layer in high performance OLEDs. *New J. Chem.* **2011**, *35*, 1534−1540.
(70) Wang, Z.; Li, X.; Xue, K.; Li, H.; Zhang, X.; Liu, Y.; Yu, Z.; Lu, P.; Chen, P. Towards stable deep-blue emission and low efficiency roll-off in OLEDs based on phenanthroimidazole dimers. *J. Mater. Chem. C* **2016**, *4*, 1886−1894.
(71) Göstl, R.; Sijbesma, R. P. π-extended anthracenes as sensitive probes for mechanical stress. *Chem. Sci.* **2016**, *7*, 370−375.
(72) Zhong, F.; Zhao, J. Phenyleneanthracene derivatives as triplet energy acceptor/emitter in red light excitable triplet-triplet-annihilation upconversion. *Dyes Pigm.* **2017**, *136*, 909−918.
(73) Zhuang, S.; Shangguan, R.; Huang, H.; Tu, G.; Wang, L.; Zhu, X. Synthesis, characterization, physical properties, and blue electroluminescent device applications of phenanthroimidazole derivatives containing anthracene or pyrene moiety. *Dyes Pigm.* **2014**, *101*, 93−102.
(74) Maus, M.; Rettig, W.; Bonafoux, D.; Lapouyade, R. Photoinduced Intramolecular Charge Transfer in a Series of Differently Twisted Donor-Acceptor Biphenyls As Revealed by Fluorescence. *J. Phys. Chem. A* **1999**, *103*, 3388−3401.
(75) Sakuda, E.; Ando, Y.; Ito, A.; Kitamura, N. Extremely Large Dipole Moment in the Excited Singlet State of Tris{[p-(N,N-dimethylamino)phenylethynyl]duryl}borane. *J. Phys. Chem. A* **2010**, *114*, 9144−9150.
(76) Ha-Thi, M.-H.; Souchon, V.; Hamdi, A.; Metivier, R.; Alain, V.; Nakatani, K.; Lacroix, P. G.; Genet, J.-P.; Michelet, V.; Leray, I. Synthesis of Novel Rod-Shaped and Star-Shaped Fluorescent Phosphane Oxides—Nonlinear Optical Properties and Photophysical Properties. *Chem. - Eur. J.* **2006**, *12*, 9056−9065.
(77) Wang, C.-L.; Lin, P.-T.; Wang, Y.-F.; Chang, C.-W.; Lin, B.-Z.; Kuo, H.-H.; Hsu, C.-W.; Tu, S.-H.; Lin, C.-Y. Cost-Effective Anthryl Dyes for Dye-Sensitized Cells under One Sun and Dim Light. *J. Phys. Chem. C* **2015**, *119*, 24282−24289.

DOI: 10.1021/acs.inorgchem.8b00422
Inorg. Chem. 2018, 57, 6349−6361

(78) Larsen, C. B.; van der Salm, H.; Shillito, G. E.; Lucas, N. T.; Gordon, K. C. Tuning the Rainbow: Systematic Modulation of Donor−Acceptor Systems through Donor Substituents and Solvent. *Inorg. Chem.* **2016**, *55*, 8446−8458.
(79) Barnsley, J. E.; Shillito, G. E.; Larsen, C. B.; van der Salm, H.; Wang, L. E.; Lucas, N. T.; Gordon, K. C. Benzo[c][1,2,5]thiadiazole Donor−Acceptor Dyes: A Synthetic, Spectroscopic, and Computational Study. *J. Phys. Chem. A* **2016**, *120*, 1853−1866.
(80) Nishida, T.; Ohta, S.; Xu, F.; Shinohara, K.; Kamada, T.; Akashi, H.; Takezaki, M.; Wakamatsu, K.; Orita, A. Dual Emission and Mechanofluorochromism of a V-Shaped π-System Composed of Disulfonyl-Substituted Dibenzocyclooctatetraenes. *Org. Lett.* **2016**, *18*, 3988−3991.
(81) Dou, K.; Chen, G.; Yu, F.; Liu, Y.; Chen, L.; Cao, Z.; Chen, T.; Li, Y.; You, J. Bright and sensitive ratiometric fluorescent probe enabling endogenous FA imaging and mechanistic exploration of indirect oxidative damage due to FA in various living systems. *Chem. Sci.* **2017**, *8*, 7851−7861.
(82) Kaljurand, I.; Kütt, A.; Sooväli, L.; Rodima, T.; Mäemets, V.; Leito, I.; Koppel, I. A. Extension of the Self-Consistent Spectrophotometric Basicity Scale in Acetonitrile to a Full Span of 28 pKa Units: Unification of Different Basicity Scales. *J. Org. Chem.* **2005**, *70*, 1019−1028.
(83) Haav, K.; Saame, J.; Kütt, A.; Leito, I. Basicity of Phosphanes and Diphosphanes in Acetonitrile. *Eur. J. Org. Chem.* **2012**, *2012*, 2167−2172.
(84) Blanco Rodríguez, A. M.; Gabrielsson, A.; Motevalli, M.; Matousek, P.; Towrie, M.; Šebera, J.; Záliš, S.; Vlček, A. J. Ligand-to-Diimine/Metal-to-Diimine Charge-Transfer Excited States of [Re(NCS)(CO)$_3$(α-diimine)] (α-diimine = 2,2′-bipyridine, di-^{i}Pr-N,N-1,4-diazabutadiene). A Spectroscopic and Computational Study. *J. Phys. Chem. A* **2005**, *109*, 5016−5025.
(85) Vlcek, A. J.; Zalis, S. Modeling of charge-transfer transitions and excited states in d6 transition metal complexes by DFT techniques. *Coord. Chem. Rev.* **2007**, *251*, 258−287.
(86) Blanco-Rodríguez, A. M.; Towrie, M.; Collin, J.-P.; Záliš, S.; Vlček, A. J. Excited-state relaxation dynamics of Re(I) tricarbonyl complexes with macrocyclic phenanthroline ligands studied by time-resolved IR spectroscopy. *Dalton Trans.* **2009**, 3941−3949.
(87) Vlček, A. J. Ultrafast Excited-State Processes in Re(I) Carbonyl-Diimine Complexes: From Excitation to Photochemistry. *Top. Organomet. Chem.* **2009**, *29*, 115−158.
(88) Záliš, S.; Milne, C. J.; El Nahhas, A.; Blanco-Rodríguez, A. M.; van der Veen, R. M.; Vlček, A. J. Re and Br X-ray Absorption Near-Edge Structure Study of the Ground and Excited States of [ReBr(CO)$_3$(bpy)] Interpreted by DFT and TDDFT Calculations. *Inorg. Chem.* **2013**, *52*, 5775−5785.
(89) Si, Z.; Li, J.; Li, B.; Zhao, F.; Liu, S.; Li, W. Synthesis, Structural Characterization, and Electrophosphorescent Properties of Rhenium(I) Complexes Containing Carrier-Transporting Groups. *Inorg. Chem.* **2007**, *46*, 6155−6163.
(90) Chu, W.-K.; Wei, X.-G.; Yiu, S.-M.; Ko, C.-C.; Lau, K.-C. Strongly Phosphorescent Neutral Rhenium(I) Isocyanoborato Complexes: Synthesis, Characterization, and Photophysical, Electrochemical, and Computational Studies. *Chem. - Eur. J.* **2015**, *21*, 2603−2612.
(91) Morimoto, T.; Ito, M.; Koike, K.; Kojima, T.; Ozeki, T.; Ishitani, O. Dual Emission from Rhenium(I) Complexes Induced by an Interligand Aromatic Interaction. *Chem. - Eur. J.* **2012**, *18*, 3292−3304.
(92) Garino, C.; Ruiu, T.; Salassa, L.; Albertino, A.; Volpi, G.; Nervi, C.; Gobetto, R.; Hardcastle, K. I. Spectroscopic and Computational Study on New Blue Emitting ReL(CO)$_3$Cl Complexes Containing Pyridylimidazo[1,5-a]pyridine Ligands. *Eur. J. Inorg. Chem.* **2008**, *2008*, 3587−3591.
(93) Salassa, L.; Garino, C.; Albertino, A.; Volpi, G.; Nervi, C.; Gobetto, R.; Hardcastle, K. I. Computational and Spectroscopic Studies of New Rhenium(I) Complexes Containing Pyridylimidazo-[1,5-α]pyridine Ligands: Charge Transfer and Dual Emission by Fine-Tuning of Excited States. *Organometallics* **2008**, *27*, 1427−1435.
(94) Bhattacharya, D. Synthesis, characterization, structure and dual room-temperature fluorescent and phosphorescent emission in μ-oxalato-bridged rhenium(I) metallacycle. *Inorg. Chem. Commun.* **2013**, *36*, 159−162.
(95) van der Salm, H.; Larsen, C. B.; McLay, J. R. W.; Fraser, M. G.; Lucas, N. T.; Gordon, K. C. Stretching the phenazine MO in dppz: the effect of phenyl and phenyl−ethynyl groups on the photophysics of Re(I) dppz complexes. *Dalton Trans.* **2014**, *43*, 17775−17785.
(96) Thorp-Greenwood, F. L.; Pritchard, V. E.; Coogan, M. P.; Hardie, M. J. Tris(rhenium fac-tricarbonyl) Polypyridine Functionalized Cyclotriguaiacylene Ligands with Rich and Varied Emission. *Organometallics* **2016**, *35*, 1632−1642.
(97) Cannizzo, A.; Blanco-Rodríguez, A. M.; El Nahhas, A.; Šebera, J.; Záliš, S.; Vlček, A. J.; Chergui, M. Femtosecond Fluorescence and Intersystem Crossing in Rhenium(I) Carbonyl-Bipyridine Complexes. *J. Am. Chem. Soc.* **2008**, *130*, 8967−8974.
(98) El Nahhas, A.; Consani, C.; Blanco-Rodríguez, A. M.; Lancaster, K. M.; Braem, O.; Cannizzo, A.; Towrie, M.; Clark, I. P.; Záliš, S.; Chergui, M.; Vlček, A. J. Ultrafast Excited-State Dynamics of Rhenium(I) Photosensitizers [Re(Cl)(CO)$_3$(N,N)] and [Re(imidazole)(CO)$_3$(N,N)]$^+$: Diimine Effects. *Inorg. Chem.* **2011**, *50*, 2932−2943.
(99) Sun, S.-S.; Lees, A. J. Self-Assembly Triangular and Square Rhenium(I) Tricarbonyl Complexes: A Comprehensive Study of Their Preparation, Electrochemistry, Photophysics, Photochemistry, and Host-Guest Properties. *J. Am. Chem. Soc.* **2000**, *122*, 8956−8967.
(100) Steffen, A.; Tay, M. G.; Batsanov, A. S.; Howard, J. A. K.; Beeby, A.; Vuong, K. Q.; Sun, X.-Z.; George, M. W.; Marder, T. B. 2,5-Bis(p-R-arylethynyl)rhodacyclopentadienes Show Intense Fluorescence: Denying the Presence of a Heavy Atom. *Angew. Chem., Int. Ed.* **2010**, *49*, 2349−2353.
(101) Blanco-Rodríguez, A. M.; Kvapilová, H.; Sýkora, J.; Towrie, M.; Nervi, C.; Volpi, G.; Záliš, S.; Vlček, A. J. Photophysics of Singlet and Triplet Intraligand Excited States in [ReCl(CO)$_3$(1-(2-pyridyl)-imidazo[1,5-α]pyridine)] Complexes. *J. Am. Chem. Soc.* **2014**, *136*, 5963−5973.
(102) Turro, N. J.; Ramamurthy, V.; Scaiano, J. C. *Modern Molecular Photochemistry of Organic Molecules*; University Science Books: Sausalito, CA, 2010.
(103) Werrett, M. V.; Muzzioli, S.; Wright, P. J.; Palazzi, A.; Raiteri, P.; Zacchini, S.; Massi, M.; Stagni, S. Proton-Induced Reversible Modulation of the Luminescent Output of Rhenium(I), Iridium(III), and Ruthenium(II) Tetrazolate Complexes. *Inorg. Chem.* **2014**, *53*, 229−243.
(104) Leasure, R. M.; Sacksteder, L.; Nesselrodt, D.; Reitz, G. A.; Demas, J. N.; DeGraff, B. A. Excited-State Acid-Base Chemistry of (α-Diimine)cyanotricarbonylrhenium(I) Complexes. *Inorg. Chem.* **1991**, *30*, 3722−3728.
(105) Heydová, R.; Gindensperger, E.; Romano, R.; Sýkora, J.; Vlček, A. J.; Záliš, S.; Daniel, C. Spin−Orbit Treatment of UV−vis Absorption Spectra and Photophysics of Rhenium(I) Carbonyl−Bipyridine Complexes: MS-CASPT2 and TD-DFT Analysis. *J. Phys. Chem. A* **2012**, *116*, 11319−11329.
(106) Gourlaouen, C.; Eng, J.; Otsuka, M.; Gindensperger, E.; Daniel, C. Quantum Chemical Interpretation of Ultrafast Luminescence Decay and Intersystem Crossings in Rhenium(I) Carbonyl Bipyridine Complexes. *J. Chem. Theory Comput.* **2015**, *11*, 99−110.
(107) Harabuchi, Y.; Eng, J.; Gindensperger, E.; Taketsugu, T.; Maeda, S.; Daniel, C. Exploring the Mechanism of Ultrafast Intersystem Crossing in Rhenium(I) Carbonyl Bipyridine Halide Complexes: Key Vibrational Modes and Spin−Vibronic Quantum Dynamics. *J. Chem. Theory Comput.* **2016**, *12*, 2335−2345.
(108) Schanze, K. S.; MacQueen, D. B.; Perkins, T. A.; Cabana, L. A. Studies of intramolecular electron and energy transfer using the *fac*-(diimine)Re^I(CO)$_3$ chromophore. *Coord. Chem. Rev.* **1993**, *122*, 63−89.

DOI: 10.1021/acs.inorgchem.8b00422
Inorg. Chem. 2018, 57, 6349−6361